https://doi.org/10.5194/nhess-2019-274
Preprint. Discussion started: 24 October 2019

An improved method of Newmark analysis for mapping hazards of coseismic landslides

Mingdong Zang [a,b,c], Shengwen Qi [a,b,c,*], Yu Zou [a,b,c], Zhuping Sheng [d], Blanca S. Zamora [d]

[a] *Key Laboratory of Shale Gas and Geoengineering, Institute of Geology and Geophysics, Chinese Academy of Sciences, Beijing 100029, China*

[b] *Institutions of Earth Science, Chinese Academy of Sciences, Beijing 100029, China*

[c] *University of Chinese Academy of Sciences, Beijing 100029, China*

[d] *Texas A&M AgriLife Research Center at El Paso, El Paso, Texas 79927, USA*

* Corresponding Author.

E-mail address: qishengwen@mail.iggcas.ac.cn (S. W. Qi)

https://doi.org/10.5194/nhess-2019-274
Preprint. Discussion started: 24 October 2019

Abstract

Coseismic landslides have been responsible for destroyed buildings and structures, dislocated roads and bridges, cut off of pipelines and lifelines, and tens of thousands of deaths. Accurately mapping the hazards of coseismic landslides is an important and challenge work. Newmark's method is widely applied to assess the permanent displacement along a potential slide surface to determine the coseismic responses of the slope. This paper considers the roughness and size effect of the potential slide surface-unloading joint, and then presents an improved method of Newmark analysis for mapping hazard of coseismic landslides. The improved method is verified using data from a case study of the 2014 M_w 6.1 (USGS) Ludian earthquake in Yunnan Province, China. The permanent displacement yielded from this method range from 0 to 122 cm. Comparisons are made between the predicted displacements and a comprehensive inventory of landslides triggered by the Ludian earthquake to map the spatial variability using certainty factor model (CFM). Confidence levels of coseismic landslides indicated by certainty factors range from -1 to 0.95. A coseismic landslide hazard map is then produced based on the spatial distribution of the values of certainty factors. Area under the curve analysis is used to draw a comparison between the improved and conventional method of Newmark analysis, revealing the improved performance of the method presented in this paper. Such method can be applied to predict the hazard zone of the region and provide guidelines for making decisions regarding infrastructure development and post-earthquake reconstruction.

Keywords: Coseismic landslide; Newmark's method; Barton model; Certainty factor; Hazard Mapping

1. Introduction

One of the major causes of landslides is recognized as the earthquake. Coseismic landslide hazards have drawn increasing attention in recent years (i.e. Jibson et al., 1998, 2000; Khazai and Sitar, 2004; Qi et al., 2010, 2011, 2012; Chen et al., 2012; Xu et al., 2013; Yuan et al., 2014). In fact, the damage caused by seismically triggered landslides is sometimes more severe than the damage direct from the earthquake (Keefer, 1984). Estimating where is likely to have slope failure under a specific shaking condition plays an important role in regional assessment of coseismic landslides.

Pseudostatic analysis formalized by Terzhagi (1950) and finite-element modeling applied by Clough and Chopra (1966) were employed to assess the seismic stability of slopes in early efforts (Jibson, 2011). Newmark (1965) first introduced a relatively simple and practical method, still commonly used, to estimate the coseismic permanent-displacements of slopes (Jibson, 2011). Studies showed that Newmark's method yields reasonable and practical results when modeling the dynamic performance of natural slopes (Wilson and Keefer, 1983; Wieczorek et al., 1985; Jibson et al., 1998, 2000; Pradel et al., 2005). Recent years, Rathje and Antonakos (2011) present a unified framework for predicting coseismic permanent sliding displacement based on Newmark's method. Chen et al. (2018) used Newmark's method to calculate the minimum accelerations required for coseismic landslides in the affected region of 2014 Ludian earthquake. Chen et al. (2019) subsequently developed an easy-operation mapping method to assess coseismic landslide hazard in the quake zone of 2014 Ludian earthquake, with the help of Newmark's method.

Such applications generally start from an analysis of the dynamic stability of slopes that is quantified as the critical acceleration. Barton model (Barton, 1973) has been widely used in rock mechanics and

https://doi.org/10.5194/nhess-2019-274
Preprint. Discussion started: 24 October 2019

engineering field to predict the shear strength of rock joints, which plays a crucial role in the calculation of critical acceleration. However, researches do not pay enough attentions on the shear strength of rock joints during the assessment of coseismic landslides. To better estimate the dynamic stability of slopes, in this paper, we introduce the Barton model (Barton, 1973) into a Newmark analysis to develop an improved modeling method for mapping hazards of coseismic landslides, using data from the 2014 Ludian earthquake in Yunnan Province, Southwestern China. As predictions of coseismic landslides are not only based on exact results, i.e., computed permanent-displacements, but also mingled with unformalized expertise (Shortliffe and Buchanan, 1975), i.e., interpreted landslides, we then present a model of inexact reasoning method, which defies analysis as applications of sets of inference rules that are expressed in the predicate logic (Shortliffe and Buchanan, 1975), to produce a coseismic landslide hazard map.

This paper briefly introduces the site characteristics and the spatial distribution of triggered landslides, describes the modeling method used for the analysis of seismic slope stability, then presents the mapping procedure of the confidence level of seismic slope-failure, and finally discusses the results of the seismic hazard assessment and the comparison with a conventional Newmark analysis.

2. Study area

The epicenter of the 2014 M_w 6.1 Ludian earthquake is located in the southeastern margin of the Tibetan plateau. A rectangular area lying immediately around the epicenter and containing dense concentrations of induced landslides was chosen for study. Elevation in the study area ranges from 785 m to 3,085 m above the sea. There are three rivers, the Niulanjiang River, the Shaba River and the Longquan River passing through the area. The topography ranges from flat in river valleys to nearly

https://doi.org/10.5194/nhess-2019-274
Preprint. Discussion started: 24 October 2019

vertical in the slopes on the side of the rivers. The Niulanjiang River, flowing from southeast (SE) to the northwest (NW), where according to Chen et al. (2015), incises down to a depth between 1,200 m and 3,300 m, resulting in about 80% of the slopes with angles greater than 40° distributed along the banks. Predominant geologic units of the study area vary in the era from Proterozoic to Mesozoic, including dolomite, limestone, shale, sandstone, basalt and slate.

A landslide inventory containing 1,416 landslides (Fig. 1) was posed by visual interpretation through comparison between pre-earthquake satellite images from Google Earth (January 30, 2014) and 0.2m-high-resolution post-earthquake aerial images (August 7, 2014, data provided by Digital Mountain and Remote Sensing Applications Center, Institute of Mountain Hazards and Environment, Chinese Academy of Sciences; Beijing Anxiang Power Technology Co., LTD.). A majority of landslides triggered in this earthquake were shallow flow-like landslides (less than 3 m deep) developing in particularly dense concentrations along steeply incised river valleys. The total area of these interpreted landslides was 7.01 km^2 within a study area of 705 km^2. A detailed study showed that 846 of the mapped landslides were greater than 1,000 m^2, occupying 6.74 km^2 and accounting for 96.1% of the total landslide area, out of which 279 of the mapped landslides were greater than 5,000 m^2, occupying 5.37 km^2 and accounting for 76.6% of the total landslide area.

3. Methodology

3.1 Modeling method

In the context of the analysis of the dynamic stability of a slope, Newmark (1965) proposed a permanent-displacement analysis that bridges the gap between simplistic pseudostatic analysis and

https://doi.org/10.5194/nhess-2019-274
Preprint. Discussion started: 24 October 2019

sophisticated, but generally impractical finite-element modeling (Jibson, 1993). Newmark's method simulates a landslide as a rigid-plastic friction block having a known critical acceleration on an inclined plane (Fig. 2), and then calculates the cumulative permanent displacement of the block as it is subjected to an acceleration-time history of an earthquake. Newmark (1965) showed that the dynamic stability of a slope is related to the critical acceleration of a potential landslide block, and it can be expressed as a simple function of the static factor of safety and the landslide geometry (Jibson et al., 1998, 2000) as below:

$$a_c = (F_S - 1) g sin\alpha \quad (1)$$

where a_c is critical acceleration in terms of g, the acceleration due to earth's gravity, F_S is static factor of safety, and α is the angle from the horizontal that the center of the slide block moves when displacement first occurs (Jibson et al., 1998, 2000). For a planar slip surface parallel to the slope, this angle can generally be approximated as the slope angle.

Natural slopes often develop a group of shallow unloading joints (Fig. 3) that parallel to the surface due to valley incisions (Gu, 1979; Hoek and Bray, 1981). Studies showed that rock slopes behave as collapsing and sliding failures of shallow unloading joints under strong earthquakes, and 90% of coseismic landslides are shallow falls and slides (Harp and Jibson, 1996; Khazai and Sitar, 2003; Dai et al., 2011; Tang et al., 2015). According to Qi et al. (2012), there are two typical kinds of earthquake triggered landslides, i.e., (a) shallow flow-like landslides with depth less than 3 m in general and (b) rock falls that are thrown by the earthquake shaking, usually occurred at the crest of the slope. For both types, the unstable rock blocks are often cut and activated along the rock joints. Therefore, the static factor of safety in terms of the critical acceleration in these conditions is related to the peak shear strength of the

https://doi.org/10.5194/nhess-2019-274
Preprint. Discussion started: 24 October 2019

rock joints. For the purpose of regional stable analysis, we use a limit-equilibrium model of an infinite slope (Fig. 2) referring to the simplification of Jibson et al. (1998, 2000) on Newmark's method. On this occasion, the value of the static factor of safety against sliding which is given by the ratio of resisting to driving force is determined by conventional analysis with no consideration of accelerations, expressed as:

$$F_S = \frac{Resisting\ force}{Driving\ force} = \frac{\tau L}{mgsin\alpha} = \frac{\tau L}{\gamma Ltsin\alpha} = \frac{\tau}{\gamma tsin\alpha} \quad (2)$$

where τ is peak shear strength of the rock joint, γ is unit weight of the rock mass, and t is the thickness of the failure rock block.

For a Newmark analysis, it has been customary to describe the shear strength of rocks not rock joints in terms of Coulomb's constants for friction and cohesion. However, both are not only stress dependent variables, but also scale dependent (Barton and Choubey, 1977). According to Barton (1973), a more satisfactory empirical relationship for predicting the peak shear strength of a joint can be written as follows:

$$\tau = \sigma_n \tan\left[JRC\ log_{10}\left(\frac{JCS}{\sigma_n}\right) + \phi_b\right] \quad (3)$$

where σ_n is effective normal stress, JRC is joint roughness coefficient, JCS is joint wall compressive strength, ϕ_b is basic friction angle, the angle of frictional sliding resistance between rock joints, which can be obtained from residual shear tests on natural joints (Barton, 1973).

The effective normal stress (σ_n) generated by the gravity acting on the rock block is as follows:

$$\sigma_n = \frac{mgcos\alpha}{L} = \frac{\gamma Ltcos\alpha}{L} = \gamma tcos\alpha \quad (4)$$

https://doi.org/10.5194/nhess-2019-274
Preprint. Discussion started: 24 October 2019

Considering the impact of size effect on JRC and JCS, formulations were developed by Barton and Bandis (1982) and are shown as below:

$$JRC_n = JRC_0 \left(\frac{L_n}{L_0}\right)^{-0.02JRC_0} \tag{5}$$

$$JCS_n = JCS_0 \left(\frac{L_n}{L_0}\right)^{-0.03JRC_0} \tag{6}$$

where the nomenclature adopted incorporates the (*0*) and (*n*) for laboratory scale and in situ scale values respectively.

Hence the static factor of safety (F_S) of a slope can be written as:

$$F_S = \frac{\tau}{\gamma t sin\alpha} = \frac{\sigma_n \tan\,[JRC_n\, log_{10}\left(\frac{JCS_n}{\sigma_n}\right) + \phi_b]}{\gamma t sin\alpha}$$
$$= \frac{\gamma t cos\alpha \tan\,[JRC_n\, log_{10}\left(\frac{JCS_n}{\gamma t cos\alpha}\right) + \phi_b]}{\gamma t sin\alpha}$$
$$= \frac{\tan\,[JRC_n\, log_{10}\left(\frac{JCS_n}{\gamma t cos\alpha}\right) + \phi_b]}{tan\alpha} \tag{7}$$

After knowing the slope angle and the static factor of safety, the critical acceleration of a slope can be determined. Once the earthquake acceleration-time history has been selected, those portions of the record lying above the critical acceleration a_c (Fig. 4a) are integrated once to derive a velocity profile (Fig. 4b), which in turn is integrated a second time to obtain the cumulative displacement profile of the block (Fig. 4c), users then judge the dynamic performance of a slope based on the magnitude of the

Newmark displacement (Jibson et al., 1998, 2000; Jibson, 2011). The detailed procedure of conducting a Newmark analysis with Barton model is discussed in the following sections.

3.2 Static factor of safety

Considering that the mapped landslides greater than 1,000 m^2 occupy 96.1% of the total landslide area, we selected a 30 m×30 m digital elevation model (DEM), ASTER Global Digital Elevation Model (https://doi.org/10.5067/ASTER/ASTGTM.002, last accessed July 16, 2018) that is capable of facilitating the subsequent hazard analysis. A basic slope algorithm was applied to the DEM to produce a slope map (Fig. 5), where the slope is identified as the steepest downhill descent from the cell to its neighbors (Burrough and McDonell, 1998). The slopes range from greater than 60° in the banks of the Niulanjiang River, the Shaba River and the Longquan River, to less than 20° in moderate and low mountains and hills in north and east.

For some slope steeper than 60°, few blocks can stay on that steep sliding surface, and the calculated F_S will be nearly zero in this case. Actually, the unstable blocks have already failed, and further sliding will occur along a failure plane inside the slope, and the angle (α) of the inclination of the failure plane will be $45°+\frac{\phi_b}{2}$. Therefore, we assigned an angle (α) of $45°+\frac{\phi_b}{2}$ to those slopes more than 60° to avoid a too low F_S in Newmark analysis.

Digital geologic map from China Geological Survey (GCS) was rasterized at 30 m grid spacing for assigning material properties throughout the study area. According to the literature researches, we found that JRC_0 and JCS_0 depend strongly on the lithology (Coulson, 1972; Barton and Choubey, 1977; Bandis et al., 1983; Priest, 1993; Bilgin and Pasamehmetoglu, 1990; Singh et al., 2012 Alejano et al., 2012, 2014; Giusepone, 2014; Yong et al., 2018). Representative values of γ, JRC_0, JCS_0 and ϕ_b

https://doi.org/10.5194/nhess-2019-274
Preprint. Discussion started: 24 October 2019

assigned to each rock type exposed in the area can normally be estimated with the help of the test data listed in Table 1. The selected values were near the middle of the ranges represented in the references. These JRC_0 and JCS_0 are considered in laboratory scale, for the length of 100 mm as L_0. For each grid cell in regional analysis, L_n, the length of engineering dimension, can generally be set as a ten-fold range of L_0, because the value of JRC_n/JRC_0 (JCS_n/JCS_0) is almost constant when the value of L_n/L_0 greater than 10 (Bandis et al., 1981). The values of JRC_n and JCS_n, then, are calculated by inserting values from JRC_0, JCS_0, L_0, and L_n into Eq. (5) and Eq. (6). Fig. 6a and Fig. 6b show the spatial distribution of JRC_n and JCS_n respectively. The basic-friction-angle (ϕ_b) map and unit weight (γ) map are shown as Fig. 7 and Fig. 8 respectively.

For simplicity, the thickness of the modeled block t was taken to be 3 m, which reflects the typical slope failures of the Ludian earthquake. The static factor-of-safety map was produced by combing these data layers (α, JRC_n, JCS_n, ϕ_b, and γ) in Eq. (7). In the initial iteration of the calculation, grid cells in steep areas with static factors of safety less than 1 indicate that the slopes are statically unstable, but do not necessarily mean that the slopes are moving under the earthquake shaking. In this condition, to avoid conservative results, we did not increase the strengths of rock types having statically unstable cells, either, adjust strengths of other rock types to preserve the relative strength differences between rock types (Jibson et al., 1998, 2000). Instead we assigned a minimal static factor of safety as 1.01, merely above limit equilibrium (Jibson et al., 1998, 2000), to these slopes, to avoid a negative value of the critical acceleration a_c. According to Keefer (1984), most landslides triggered by earthquakes occur with a slope of 5° at least. Static factors of safety resulting from slopes less than 5° were very high, and these slopes that were impossible to have failures under the Ludian earthquake did not produce a statistically significant sample

https://doi.org/10.5194/nhess-2019-274
Preprint. Discussion started: 24 October 2019

to the analysis. Therefore, slopes less than 5° were not analyzed during the second iteration. After the adjustment, the static factors of safety ranged from 1.0 to 17.4, as shown in Fig. 9.

3.3 Critical acceleration

According to Newmark (1965), a pseudostatic analysis in terms of the static factor of safety and the slope angle was employed to calculate the critical acceleration of a potential landslide. The critical-acceleration map (Fig. 10) was produced by combining the static factor of safety and the slope angle in Eq. (1).

The critical acceleration that results in a static factor of safety of 1.0 and initiates a sliding of a slope in a limit-equilibrium analysis is derived from the intrinsic slope properties (topography and lithology), regardless which ground shaking is given. Therefore, the critical-acceleration map indicates the susceptibility of the coseismic landslides (Jibson et al., 1998, 2000). The calculated critical accelerations range from almost zero in areas that are more susceptible to coseismic landslides, to 14.0 g in areas with lower susceptibility.

3.4 Shake map

There are 23 strong-motion stations within 100 km of the Ludian earthquake epicenter (Fig. 11). Each station record includes three components of the peak ground acceleration (PGA), in south-north direction, east-west direction and up-down direction respectively, as listed in Table 2 (The data set is provided by China Earthquake Data Center, http://data.earthquake.cn, last accessed June 16, 2016). We calculated the average PGA of the two horizontal components of each strong-motion recording, and then plotted a contour map (Fig. 12) using an Inverse Distance Weighted (IDW) interpolation algorithm. This method assumes that the variable of the average PGA being mapped decreases in influence with distance from its sampled location. Inverse Distance Weighted (IDW) interpolation determines cell values using a linearly weighted combination of a set of sample stations (Watson and Philip, 1985). The weight is a function of inverse distance. In addition, considering that input stations far away from the epicenter location where the prediction is being made may have poor or no spatial correlation, we eliminated the input stations out of 100 km from the calculation.

3.5 Newmark displacement

In a real landslide hazard case, it is impossible to conduct a rigorous Newmark analysis when accelerometer records are unavailable. It is also impractical and time consuming to produce a displacement in each cell during the regional analysis. Therefore, empirical regressions (Ambraseys and Menu, 1988; Bray and Travasarou, 2007; Jibson, 2007; Saygili and Rathje, 2008; Rathje and Saygili, 2009; Hsieh and Lee, 2011) were proposed to estimate Newmark displacement as a function of the critical acceleration and peak ground acceleration or Arias intensity. Among those empirical estimations, Rathje and Saygili (2009) developed a vector model for displacement in terms of the critical acceleration (a_c), peak ground acceleration (PGA) and moment magnitude (M_w) based on analysis of over 2,000 strong motions.

$$lnD = 4.89 - 4.85\left(\frac{a_c}{PGA}\right) - 19.64\left(\frac{a_c}{PGA}\right)^2 + 42.49\left(\frac{a_c}{PGA}\right)^3 - 29.06\left(\frac{a_c}{PGA}\right)^4 + 0.72\ln(PGA) + 0.89(M_w - 6) \tag{8}$$

where D is predicted displacement in units of cm, a_c and PGA are in units of g.

This model is a preferred displacement model at a specific site where acceleration-time recordings are not available. The incorporating multiple ground motion parameters in the analysis typically results in less variability in the prediction of displacement (Rathje and Saygili, 2009).

The Newmark displacement (Fig. 13) in each cell was calculated by combing corresponding values of the critical acceleration, peak ground acceleration and moment magnitude in Eq (8). Predicted displacements range from 0 cm to 122 cm.

3.6 Certainty factor and coseismic landslide hazard map

According to Jibson et al. (1998, 2000), predicted displacements provide an index of seismic performance of slopes, larger predicted displacements relate to greater incidence of slope failures. But the displacements do not correspond directly to measurable slope movements in the field. To produce a coseismic landslide hazard map, we chose a model of inexact reasoning, the certainty factor model (CFM), which was created by Shortliffe and Buchanan (1975) and improved by Hecherman (1986), to explore the relationship between the landslide occurrences and the predicted displacements. The CFM was created as a numerical method, which was initially used by MYCIN, a backward chaining expert system in medicine (Shortliffe and Buchanan, 1975), for managing uncertainty in a rule-based system. In this model, the certainty factor CF represents the net confidence in a hypothesis H based on the evidence E (Hecherman, 1986). Certainty factors range between -1 and 1. A CF with a value of -1 means total lack of confidence, whereas a CF with a value of 1 means total confidence. Values greater than 0 favor the hypothesis while values less than 0 favor the negation of the hypothesis. According to Hecherman (1986), there is a probabilistic interpretation for CF shown as below:

$$CF = \begin{cases} \dfrac{p(H|E) - p(H)}{p(H|E)[1 - p(H)]}, & p(H|E) > p(H) \\ \dfrac{p(H|E) - p(H)}{p(H)[1 - p(H|E)]}, & p(H|E) < p(H) \end{cases} \tag{9}$$

where CF is the certainty factor, $p(H|E)$ denotes the conditional probability for the case of a posterior hypothesis that relies on evidence, the posterior probability, and $p(H)$ is the prior probability before any evidence is known. In the displacement analysis, $p(H|E)$ was defined as the proportion of the landslide area within a specific displacement area while $p(H)$ was defined as the proportion of the landslide area within the entire study area excluding the slopes less than 5°. In this way, values of CF represent the confidence level of coseismic landslides. Positive values correspond to an increase in confidence level in a slope failure while negative quantities correspond to a decrease in confidence level. Greater positive values indicate higher confidence level of coseismic landslides.

Given this definition, we could produce a coseismic landslide hazard map in terms of certainty factors. First, displacement cells in every 1 cm were grouped into bins, such that all cells having displacements between 0 cm and 1 cm were grouped into the first bin; those having displacements between 1 cm and 2 cm were grouped into the second bin, and so on. The displacements were grouped into 123 bins, from 0 cm to 122 cm. Later, we calculated the proportion of cells occupied by landslide area in each bin. This proportion was considered the posterior probability of each bin as defined. The prior probability calculated by dividing the entire landslide area by the entire study area is same in each bin. Finally, values of CF were computed in each bin by using Eq. (9) to combine corresponding values of the posterior probability and prior probability. Certainty factors range from -1 to 0.95. Values of CF indicate the confidence level of landslide occurrence of each bin in the study area and provide the basis for producing a coseismic landslide hazard map.

As shown in the hazard map for the Ludian earthquake (Fig. 14), most of the actual triggered landslides lie in the higher confidence-level areas with CF values greater than 0.60. The interpreted landslides are covered on the map to demonstrate the good fit for predicted confidence levels of coseismic landslides.

4. Results and Discussion

The predicted displacements represent the cumulative sliding displacements for a given acceleration-time history. Based on the statistically significant sizes of the area of each displacement, displacements less than 60 cm, which is around the middle of the displacement range, occupy about 80% of the study area, while displacements greater than 80 cm occupy a very small area. Jibson et al. (1998, 2000) supposed that shallow falls and slides in brittle, weakly cemented materials would fail at a relatively small displacement, while slumps and block slides in more compliant materials would likely fail at a larger displacement. That is to say, the study area is more susceptible to rock falls and shallow, disrupted slides that fail at a relatively small displacement, while the study area is with a lower probability subjected to coherent, deep-seated slides that would fail at a larger displacement. Indeed, the majority of landslides triggered by the Ludian earthquake were shallow, disrupted slides and rock falls (Zhou et al., 2016). Although few catastrophic rock avalanches, such as the Hongshiyan landslide (Chang et al., 2017), occurred in the field, they did not produce statistically significant samples that could meaningfully contribute to the model, which was consistent with the statistic results as discussed previously. Therefore, the model should relate well to typical kinds of earthquake-induced landslides in the study area, meanwhile demonstrate its potential utility to predict the probability of other types of landslides.

For each CF-value area, the proportion of area occupied by landslide area was plotted as a dot in Fig. 15. The data was fitted by a piecewise function, which was derived from Eq. (9). Different from a Weibull curve (1939) through statistical regression, whose shape would probably be different in different regions (Jibson et al., 1998, 2000), the piecewise function of CF value and the proportion of landslide area can be derived from Eq. (9). This method is more universal. From the curve shown in Fig. 15, when the value of CF is reaching 1.0 (total confidence), the proportion of landslide area is trending to monotonically increase, which means the confidence level of a slope failure is growing and a landslide would probably occur. Such a procedure is consistent with the interpretation of the certainty factor theory. Therefore, the CFM demonstrates the capability of its representation and predicting approach for a probabilistic hazard analysis of coseismic landslides.

When fitting the results of shear tests using Coulomb's linear relation, the shear strengths vary widely from high normal stress in laboratory to low normal stress in the field (Barton, 1973). We introduced Barton model into the Newmark analysis to reduce the variability of shear strengths in terms of Coulomb's constants. And we considered the impact of scale effects by using Eq. (5) and Eq. (6), which helps to prevent Newmark's method from underestimating the shear strength of geologic units in a regional analysis. In addition, for Barton model, the joint roughness coefficient (JRC) could be estimated from tilt tests or from matching of Barton joint standard roughness profiles that were regarded by the International Society for Rock Mechanics (ISRM, 1978), while the joint wall compressive strength (JCS) could be estimated by Schmidt hammer index tests. These tests are helpful to make a quick estimate of the shear

https://doi.org/10.5194/nhess-2019-274
Preprint. Discussion started: 24 October 2019

strength in situ, which could facilitate using Newmark's method in an emergency hazard and risk assessment after an earthquake.

It is difficult for a statically stable slope to fail under an earthquake. Earthquakes usually make statically unstable slopes or slopes on the boundary fail. For this reason, it is important to truthfully characterize the shear strengths of slopes. Shear strengths assigned to the geologic units were from results of hundreds of shear tests from the references. We assigned the original shear strengths to the geologic units other than increasing strengths to make statically unstable cells stable as Jibson et al. (1998, 200) did, which will change the statically stable level of the whole area, especially the slopes on the boundary at first. In addition, we considered size effect of the potential slide surface, this would yield lower F_S, which, in turn, yield higher displacement. However, the actual inventory of landslides was used to calibrate the predicted displacements, and the confidence levels indicated by certainty factors fit well of the spatial distribution of coseismic landslides as shown in the hazard map (Fig. 14).

We also ran a conventional Newmark analysis using assigned strengths, such as internal friction angle (φ) and cohesion (c) as shown in Table 2. Predicted displacements calculated by the conventional Newmark analysis range from 0 cm to 121 cm, compared with 0 cm to 122 cm by the new method described in the paper. Fig. 16 shows the hazard map produced using the conventional Newmark analysis. The CFs range from -1 to 0.94, almost the same as results from the new method above. However, there are big differences along the Shaba River and upstream of the Niulanjiang River from these two methods. By comparing Fig. 14 with Fig. 16, we can see that confidence levels from the new method fit better than that of the conventional method, especially near upstream of the Niulanjiang River. The area under the curve (AUC) analysis was employed to compare performances of both methods. To create an AUC plot, the cumulative area of CFs within each interval of calculated values from the maximum to the minimum was determined as a proportion of the total study area (x-axis) and plotted against the proportion of cumulative landslides falling within those CFs (y-axis) (Miles and Keefer, 2009). The area under the curve is calculated as an index to conduct comparison across both methods. A value of 0.5 indicates performance that is no better than random guessing and 1.0 indicates perfect performance (Miles and Keefer, 2009). Fig. 17 shows the results of the AUC analysis for both methods. The calculated AUC value for the new method is 0.58, while the value for the conventional Newmark's method is 0.53. That is to say, the new method introduced in this paper yields better results, and it is actually an improvement over the conventional way of Newmark analysis.

5. Conclusion

Newmark's method is a useful, physically based model to estimate the seismic stability of natural slopes. Mapping procedure of data from the 2014 Ludian earthquake shows the feasibility of a Newmark analysis combined with Barton' shear strength criterion. Such method provides practical applications in regional seismic hazard assessment. We also consider the size effect of shear strength parameters, such as the joint roughness coefficient (JRC) and the joint wall compressive strength (JCS) in a regional analysis. Moreover, the linkage of Newmark displacements to certainty factor model improves the utility of Newmark's method to predict the hazard of coseismic landslides. Finally, results of the AUC analysis indicate that the new method has higher reliability than a conventional Newmark's method.

Acknowledgements

https://doi.org/10.5194/nhess-2019-274
Preprint. Discussion started: 24 October 2019

This work is supported by Natural Science Foundation of China under Grants of Nos. 41825018 and 41672307, Science and Technology Service Network Initiative under Grant No. KFJ-EW-STS-094, and the sponsorship from the China Scholarship Council (No. 201704910537).

References

Alejano, L. R., González, J. and Muralha, J.: Comparison of different techniques of tilt testing and basic friction angle variability assessment. Rock mechanics and rock engineering 45(6), 1023-1035, 2012.

Alejano, L. R., Perucho, Á., Olalla, C. and Jiménez, R.: Rock engineering and rock mechanics: structures in and on rock masses. CRC Press, Boca Raton, Florida, 615-1148, 2014.

Ambraseys, N. N. and Menu, J. M.: Earthquake‐induced ground displacements. Earthquake engineering and structural dynamics 16(7), 985-1006, 1988.

Bandis, S., Lumsden, A. C. and Barton, N. R.: Experimental studies of scale effects on the shear behaviour of rock joints. International Journal of Rock Mechanics and Mining Sciences & Geomechanics Abstracts 18(1), 1-21, 1981.

Bandis, S. C., Lumsden, A. C. and Barton, N. R.: Fundamentals of rock joint deformation. International Journal of Rock Mechanics and Mining Sciences & Geomechanics Abstracts 20(6), 249-268, 1983.

Barton, N.: Review of a new shear-strength criterion for rock joints. Engineering geology 7(4), 287-332, 1973.

Barton, N. and Bandis, S.: Effects of block size on the shear behavior of jointed rock. Keynote Lecture in the 23rd US Symposium on Rock Mechanics (USRMS). American Rock Mechanics Association, Berkeley, California, 739-760, 1982.

Barton, N. and Choubey, V.: The shear strength of rock joints in theory and practice. Rock mechanics 10(1-2), 1-54, 1977.

Bilgin, H. A. and Pasamehmetoglu, A. G.: Shear behaviour of shale joints under heat in direct shear. In Barton N. and Stephansson O. (Eds.), Rock joints. CRC Press, Rotterdam, 179-183, 1990.

Bray, J. D. and Travasarou, T.: Simplified procedure for estimating earthquake-induced deviatoric slope displacements. Journal of geotechnical and geoenvironmental engineering 133(4), 381-92, 2007.

Burrough, P. A. and McDonnell, R. A.: Principles of geographical information systems (2nd Edition). Oxford University Press, New York, 190, 1998.

Chang, Z. F., Chang, H., Yang, S. Y., Chen, G. and Li, J. L.: Characteristics and formation mechanism of large rock avalanches triggered by the Ludian Ms6.5 earthquake at Hongshiyan and Ganjiazhai. Seismology and Geology 39(5), 1030-1047, 2017 (in Chinese with English abstract).

Chen, X. L., Ran, H. L. and Yang, W. T.: Evaluation of factors controlling large earthquake-induced landslides by the Wenchuan earthquake. Natural Hazards and Earth System Sciences, 12(12), 3645-3657, 2012.

Chen, X. L., Zhou, Q. and Liu, C. G.: Distribution pattern of coseismic landslides triggered by the 2014 Ludian, Yunnan, China Mw6.1 earthquake: special controlling conditions of local topography. Landslides 12(6), 1159-1168, 2015.

Chen, X. L., Liu, C. G., Wang, M. M. and Zhou, Q.: Causes of unusual distribution of coseismic landslides triggered by the Mw 6.1 2014 Ludian, Yunnan, China earthquake. Journal of Asian Earth Sciences 159, 17-23, 2018.

Chen, X. L., Liu, C. G. and Wang, M. M.: A method for quick assessment of earthquake-triggered landslide hazards: a case study of the Mw6. 1 2014 Ludian, China earthquake. Bulletin of Engineering Geology and the Environment 78(4), 2449-2458, 2019.

Clough, R. W. and Chopra, A. K.: Earthquake stress analysis in earth dams. ASCE Journal of the Engineering Mechanics Division 92, 197-211, 1966.

Coulson, J.H.: Shear strength of flat surfaces in rock. In Cording, E. J. (Ed.), Stability of Rock Slopes. 13th Symposium on Rock Mechanics, Urbana, Illinois, 77-105, 1972.

Dai, F. C., Xu, C., Yao, X., Xu, L., Tu, X. B. and Gong, Q. M.: Spatial distribution of landslides triggered by the 2008 Ms 8.0 Wenchuan earthquake, China. Journal of Asian Earth Sciences 40(4), 883-895, 2011.

Geological Engineering Handbook Editorial Committee: Geological Engineering Handbook. China Architecture & Building Press, Beijing, 2018 (in Chinese).

Giusepone, F. and da Silva, L. A. A.: Hoek & Brown and Barton & Bandis Criteria Applied to a Planar Sliding at a Dolomite Mine in Gandarela Synclinal. In ISRM Conference on Rock Mechanics for Natural Resources and Infrastructure-SBMR 2014. International Society for Rock Mechanics, 2014.

Gu, D. Z.: Engineering geomechanics of rock mass. Science Press, Beijing, China, 1979 (in Chinese).

Harp, E. L. and Jibson, R. W.: Landslides triggered by the 1994 Northridge, California, earthquake. Bulletin of the Seismological Society of America 86(1B), S319-S332, 1996.

Heckerman, D.: Probabilistic interpretations for MYCIN's certainty factors. In Kanal, L. N. and Lemmer, J. F. (Eds), Machine Intelligence and Pattern Recognition 4, North-Holland, 167-196, 1986.

Hsieh, S. Y. and Lee, C. T.: Empirical estimation of the Newmark displacement from the Arias intensity and critical acceleration. Engineering Geology 122(1-2), 34-42, 2011.

Hoek, E. and Bray, J. D.: Rock slope engineering. CRC Press, 1981.

ISRM (International Society for Rock Mechanics): Suggested Methods for the Quantitative Description of Discontinuities in Rock Masses. International Journal of Rock Mechanics and Mining Sciences & Geomechanics Abstracts 15, 319-368, 1978.

Jibson, R. W.: Predicting earthquake-induced landslide displacements using Newmark's sliding block analysis. Transportation research record 1411, 9-17, 1993.

Jibson, R. W.: Methods for assessing the stability of slopes during earthquakes-A retrospective. Engineering Geology, 122(1-2), 43-50, 2011.

Jibson, R. W.: Regression models for estimating coseismic landslide displacement. Engineering Geology 91(2), 209-218, 2007.

Jibson, R. W., Harp, E. L. and Michael, J. A.: A method for producing digital probabilistic seismic landslide hazard maps: an example from the Los Angeles, California, area. US Geological Survey. Open-File Rep. 98-113. 17 pp., 1998.

Jibson, R. W., Harp, E. L. and Michael, J. A.: A method for producing digital probabilistic seismic landslide hazard maps. Engineering Geology 58(3-4), 271-289, 2000.

Keefer, D. K.: Landslides caused by earthquakes. Geological Society of America Bulletin 95(4), 406-421, 1984.

Khazai, B. and Sitar, N.: Evaluation of factors controlling earthquake-induced landslides caused by Chi-Chi earthquake and comparison with the Northridge and Loma Prieta events. Engineering geology 71(1-2), 79-95, 2004.

Miles, S. B. and Keefer, D. K.: Evaluation of CAMEL-comprehensive areal model of earthquake-induced landslides. Engineering Geology 104(1-2), 1-15, 2009.

NASA/METI/AIST/Japan Spacesystems and U.S./Japan ASTER Science Team: ASTER Global Digital Elevation Model version 2. NASA EOSDIS Land Processes DAAC, https://doi: 10.5067/ASTER/ASTGTM.002 (last accessed July 16, 2018), 2009.

Newmark, N. M.: Effects of earthquakes on dams and embankments. Geotechnique 15(2), 139-160, 1965.

Pradel, D., Smith, P. M., Stewart, J. P. and Raad, G.: Case history of landslide movement during the Northridge earthquake. Journal of Geotechnical and Geoenvironmental Engineering 131(11), 1360-1369, 2005.

Priest, S. D.: Discontinuity analysis for rock engineering. Springer Science & Business Media, B.V., Dordrecht, 320, 2012.

Qi, S. W., Xu, Q., Lan, H. X., Zhang, B. and Liu, J. Y.: Spatial distribution analysis of landslides triggered by 2008.5.12 Wenchuan Earthquake, China, Engineering Geology 116 (1-2), 95~108, 2010.

Qi, S. W., Xu, Q., Zhang, B., Zhou, Y. D., Lan, H. X. and Li, L. H.: Source characteristics of long runout rock avalanches triggered by the 2008 Wenchuan earthquake, China, Journal of Asian Earth Sciences 40 (4), 896~906, 2011.

Qi, S. W., Yan, C. G. and Liu, C. L.: Two typical types of earthquake triggered landslides and their mechanisms. In Landslides and Engineered Slopes: Protecting Society through Improved Understanding, ISBN 978-0-415-63303-1, 2012.

Rathje, E. M. and Antonakos, G.: A unified model for predicting earthquake-induced sliding displacements of rigid and flexible slopes. Engineering Geology 122(1-2), 51-60, 2011.

Rathje, E. M. and Saygili, G.: Probabilistic assessment of earthquake-induced sliding displacements of natural slopes. Bulletin of the New Zealand Society for Earthquake Engineering 42(1), 18-27, 2009.

Saygili, G. and Rathje, E. M.: Empirical predictive models for earthquake-induced sliding displacements of slopes. Journal of Geotechnical and Geoenvironmental Engineering 134(6), 790-803, 2008.

Shortliffe, E. H. and Buchanan, B. G.: A model of inexact reasoning in medicine. Mathematical Biosciences 23, 351-379, 1975.

Singh, T. N., Kainthola, A. and Venkatesh, A.: Correlation between point load index and uniaxial compressive strength for different rock types. Rock Mechanics and Rock Engineering 45(2), 259-264, 2012.

Tang, C., Ma, G., Chang, M., Li, W., Zhang, D., Jia, T. and Zhou, Z.: Landslides triggered by the 20 April 2013 Lushan earthquake, Sichuan Province, China. Engineering Geology 187, 45-55, 2015.

Terzhagi, K.: Mechanism of landslides. In Paige, S. (Ed.), Application of Geology to Engineering Practice (Berkey Volume). Geological Society of America, New York, NY, 83-123, 1950.

Watson, D. F. and Philip, G. M.: A Refinement of Inverse Distance Weighted Interpolation. Geoprocessing 2, 315–327, 1985.

Weibull, W.: In: A Statistical Theory of the Strength of Materials. Ingenioersvetenskaps-akademien, Handlingar, Stockholm, p., 151, 1939.

Wieczorek, G. F., Wilson, R. C. and Harp, E. L.: Map showing slope stability during earthquakes in San Mateo County, California. U.S. Geological Survey Miscellaneous Investigations Map I-1257-E, scale 1:62,500, 1985.

Wilson, R. C. and Keefer, D. K.: Dynamic analysis of a slope failure from the 6 August 1979 Coyote Lake, California, earthquake. Bulletin of the Seismological Society of America 73(3), 863-877, 1983.

Xu, C., Xu, X., Zhou, B., amd Yu, G.: Revisions of the M 8.0 Wenchuan earthquake seismic intensity map based on co-seismic landslide abundance. Natural Hazards, 69(3), 1459-1476, 2013.

https://doi.org/10.5194/nhess-2019-274
Preprint. Discussion started: 24 October 2019

Yong, R., Ye, J., Liang, Q. F., Huang, M. and Du, S. G.: Estimation of the joint roughness coefficient (JRC) of rock joints by vector similarity measures. Bulletin of Engineering Geology and the Environment 77, 735-749, 2018.

Yuan, R. M., Tang, C. L., Hu, J. C., and Xu, X. W.: Mechanism of the Donghekou landslide triggered by the 2008 Wenchuan earthquake revealed by discrete element modeling. Natural Hazards and Earth System Sciences, 14(5), 1195-1205, 2014.

Zhou, S. H., Chen, G. Q. and Fang, L. G.: Distribution pattern of landslides triggered by the 2014 Ludian earthquake of China: Implications for regional threshold topography and the seismogenic fault identification. ISPRS International Journal of Geo-Information 5(4), 46, 2016.

Figure Captions

Fig. 1. Map of the study area showing interpreted landslides.

Fig. 2. Conceptual sliding-block model of a Newmark analysis.

Fig. 3. A schematic diagram showing shadow unloading joints in the slope.

Fig. 4. Demonstration of the Newmark-analysis algorithm (adapted from Wilson and Keefer, 1983; Jibson et al., 1998, 2000)

Fig. 5. Slope map derived from the DEM of the study area.

Fig. 6. (a) JRC_n component and (b) JCS_n component of shear strength assigned to rock types in the study area.

Fig. 7. Basic-friction-angle (ϕ_b) component of shear strength assigned to rock types in the study area.

Fig. 8. Unit weight (γ) assigned to rock types in the study area.

Fig. 9. Static factor-of-safety map of the study area.

Fig. 10. Map showing critical accelerations in the study area.

Fig. 11. Locations of strong-motion stations.

Fig. 12. Contour map of peak ground acceleration (PGA) produced by the Ludian earthquake in the study area. PGA values shown are in g.

Fig. 13. Map showing predicted displacements in the study area.

Fig. 14. Map showing confidence levels of coseismic landslides in the Ludian earthquake using method introduced in this paper. Confidence levels are portrayed in terms of values of CF.

https://doi.org/10.5194/nhess-2019-274
Preprint. Discussion started: 24 October 2019

Fig. 15. Proportion of the area of landslides lying in each CF-value area. A dot shows the proportion of landslide area within an area of CF value; the red line is the fitting curve of the data using second order exponential growth function.

Fig. 16. Map showing confidence levels of coseismic landslides in the Ludian earthquake using a conventional Newmark analysis. Confidence levels are portrayed in terms of values of CF.

Fig. 17. Area under the curve plots for comparing the new method with a conventional Newmark's method.

https://doi.org/10.5194/nhess-2019-274
Preprint. Discussion started: 24 October 2019

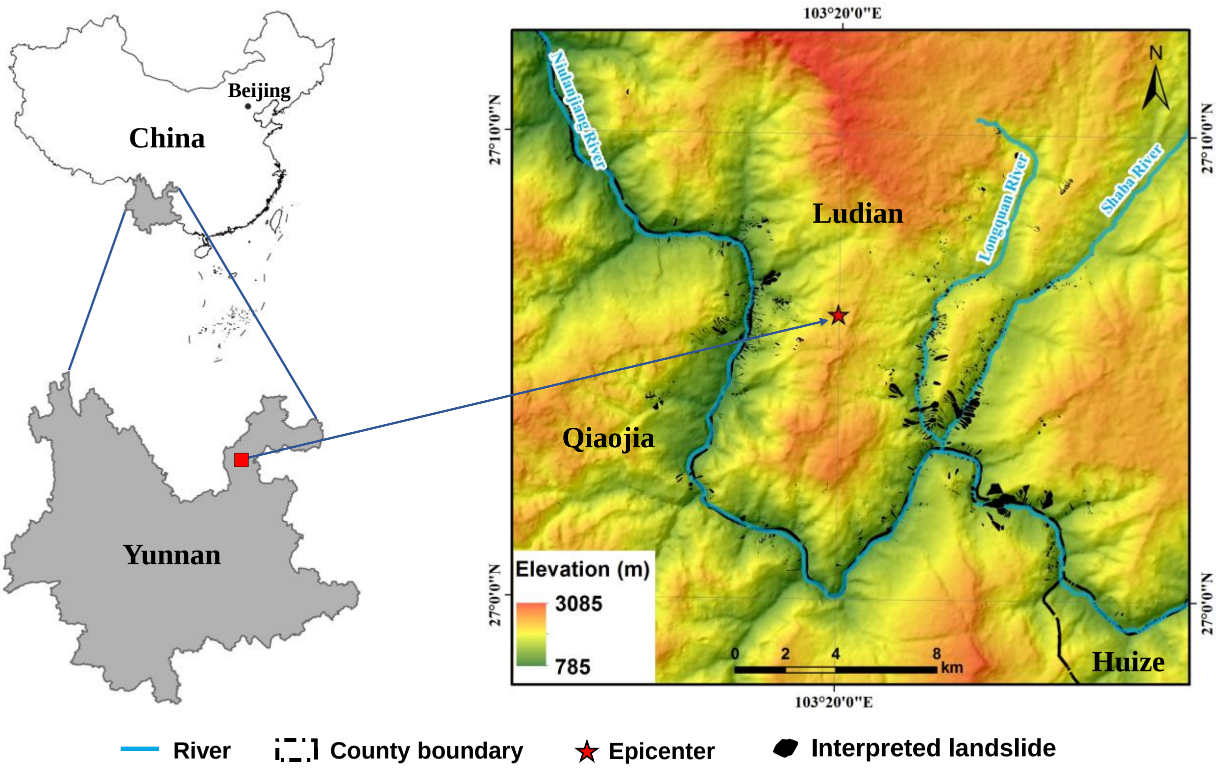

Fig. 1. Map of the study area showing interpreted landslides.

https://doi.org/10.5194/nhess-2019-274
Preprint. Discussion started: 24 October 2019

Natural Hazards and Earth System Sciences
Open Access
EGU
Discussions

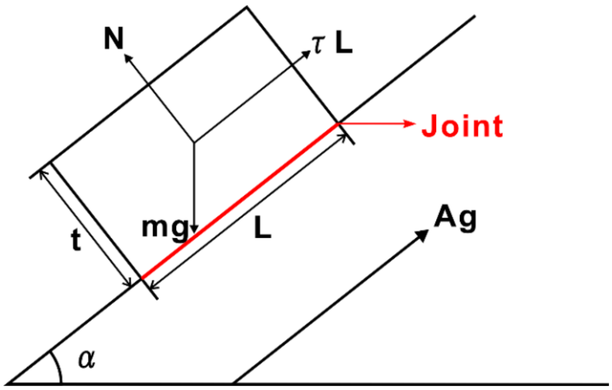

Fig. 2. Conceptual sliding-block model of a Newmark analysis. The potential landslide is modeled as a rigid-plastic block resting on an inclined plane at an angle (α) from the horizontal (Jibson et al., 1998, 2000). The base of the block is subjected to an earthquake ground acceleration that is denoted by Ag.

https://doi.org/10.5194/nhess-2019-274
Preprint. Discussion started: 24 October 2019

Natural Hazards and Earth System Sciences
Discussions

516 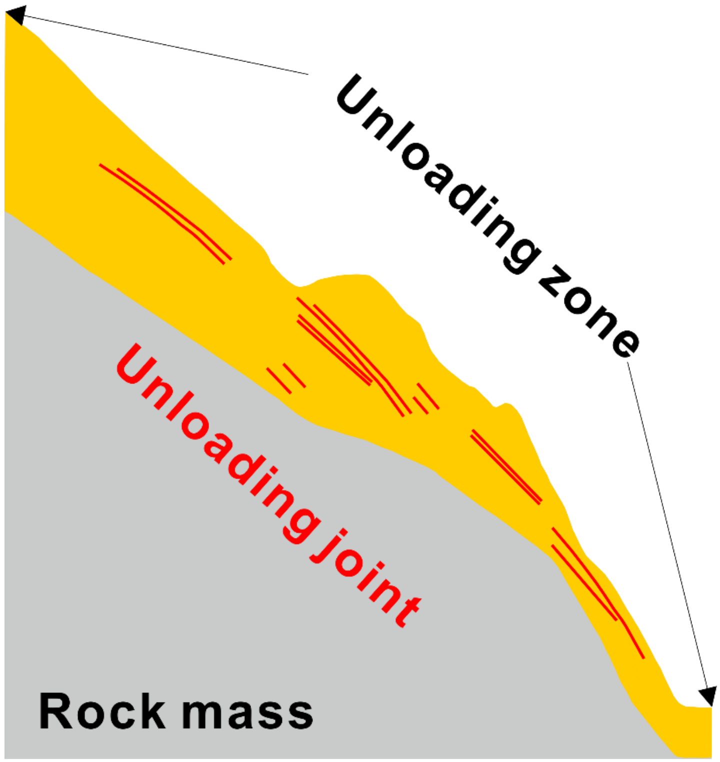

517 **Fig. 3.** A schematic diagram showing shallow unloading joints in the slope.

518

https://doi.org/10.5194/nhess-2019-274
Preprint. Discussion started: 24 October 2019

Natural Hazards and Earth System Sciences
Discussions

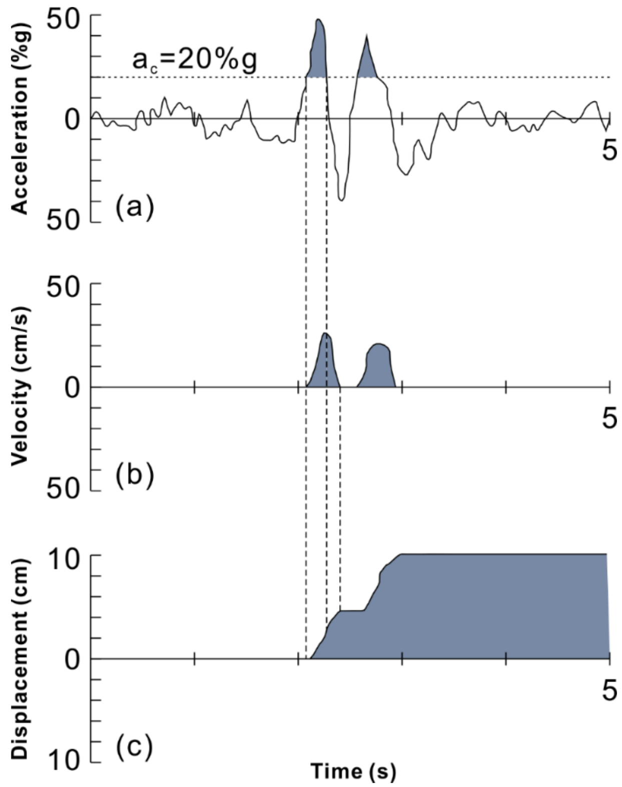

Fig. 4. Demonstration of the Newmark-analysis algorithm (adapted from Wilson and Keefer, 1983; Jibson et al., 1998, 2000): (a) Acceleration-time history with critical acceleration (horizontal dotted line) of 20%g superimposed. (b) Velocity of block versus time. (c) Displacement of block versus time.

https://doi.org/10.5194/nhess-2019-274
Preprint. Discussion started: 24 October 2019

Natural Hazards and Earth System Sciences
Open Access
EGU
Discussions

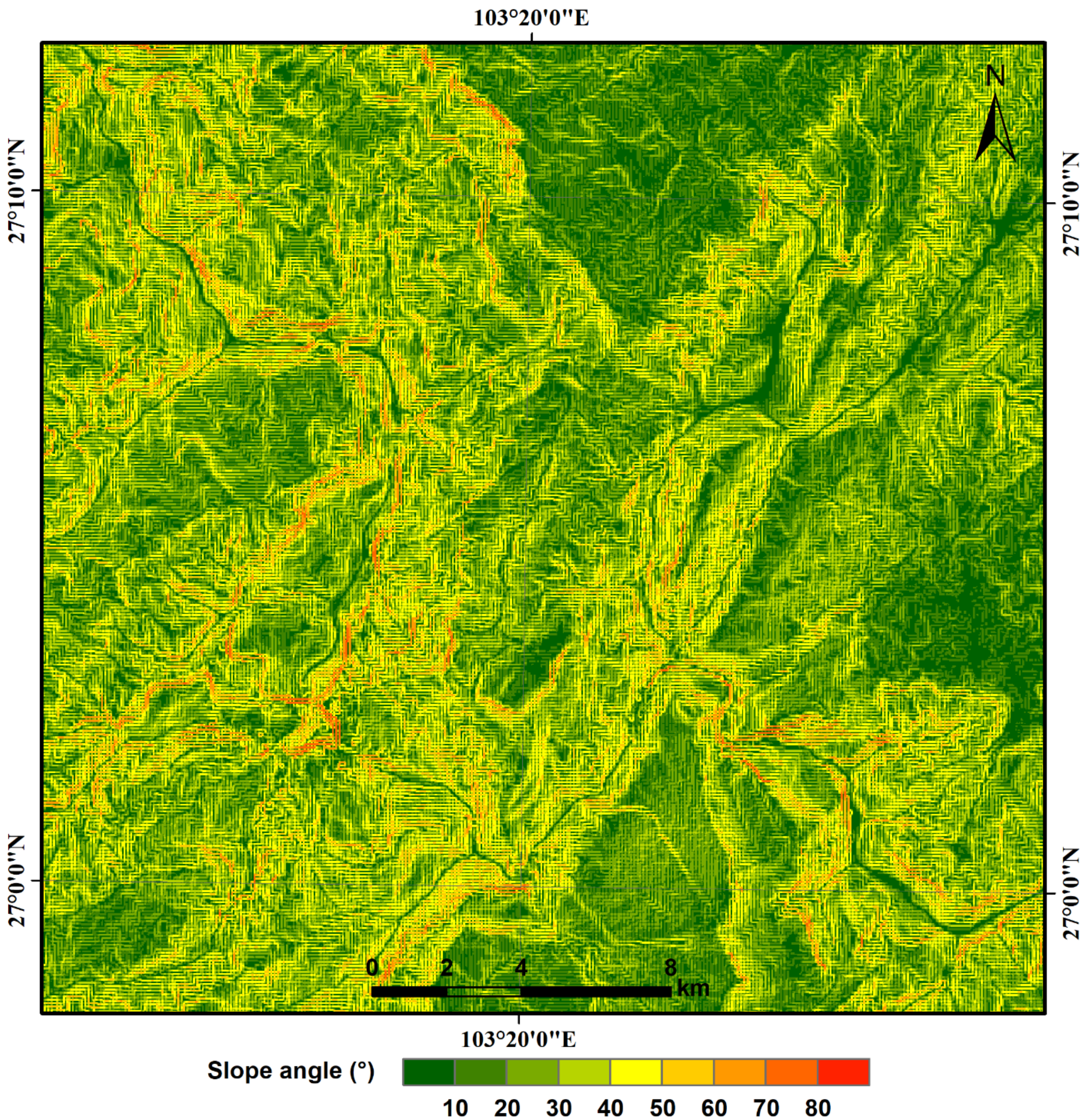

Fig. 5. Slope map derived from the DEM of the study area.

https://doi.org/10.5194/nhess-2019-274
Preprint. Discussion started: 24 October 2019

Natural Hazards and Earth System Sciences
Open Access
EGU
Discussions

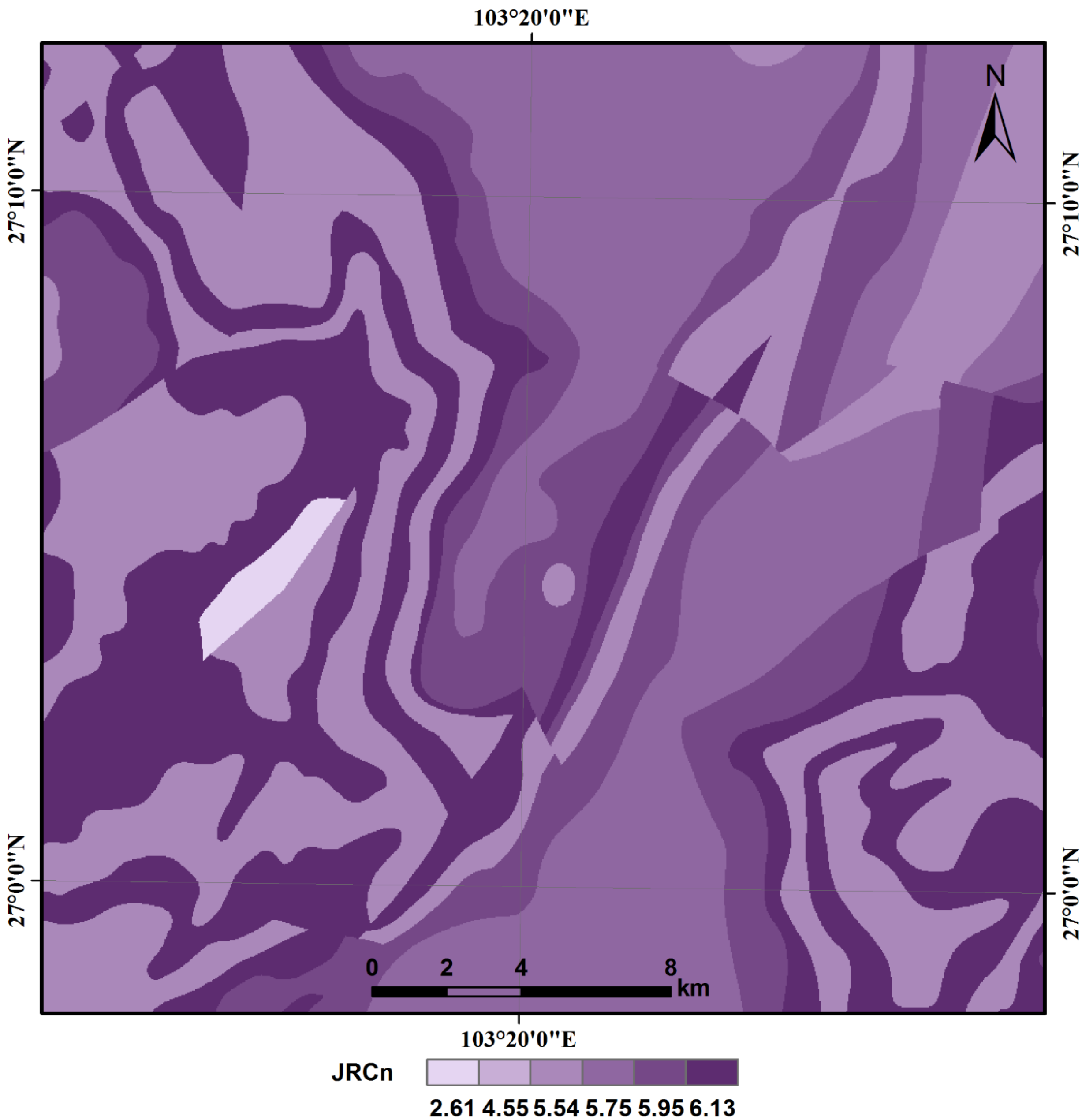

(a)

https://doi.org/10.5194/nhess-2019-274
Preprint. Discussion started: 24 October 2019

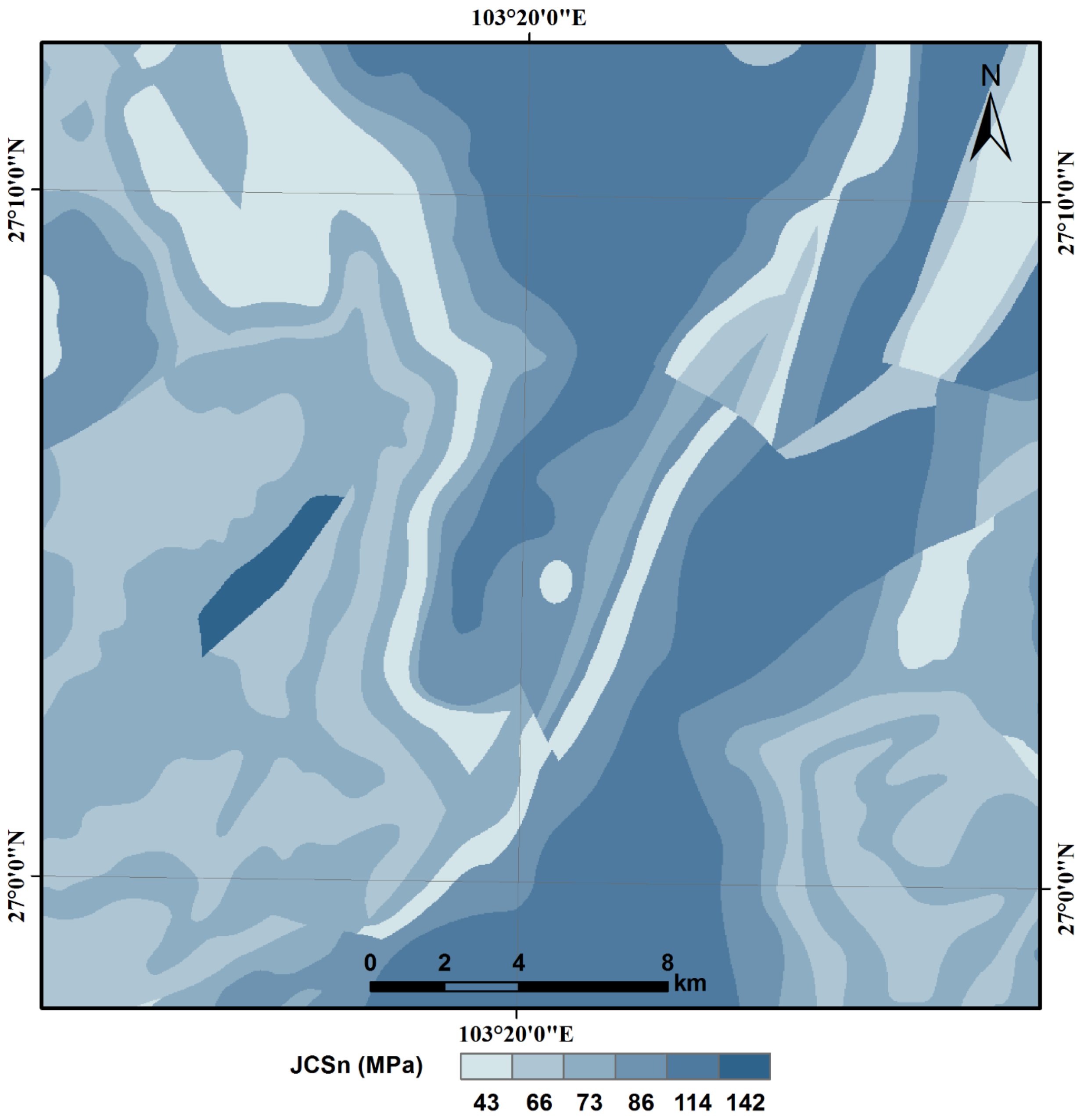

(b)

Fig. 6. (a) JRC_n component and (b) JCS_n component of shear strength assigned to rock types in the study area.

https://doi.org/10.5194/nhess-2019-274
Preprint. Discussion started: 24 October 2019

Natural Hazards and Earth System Sciences
Open Access
Discussions

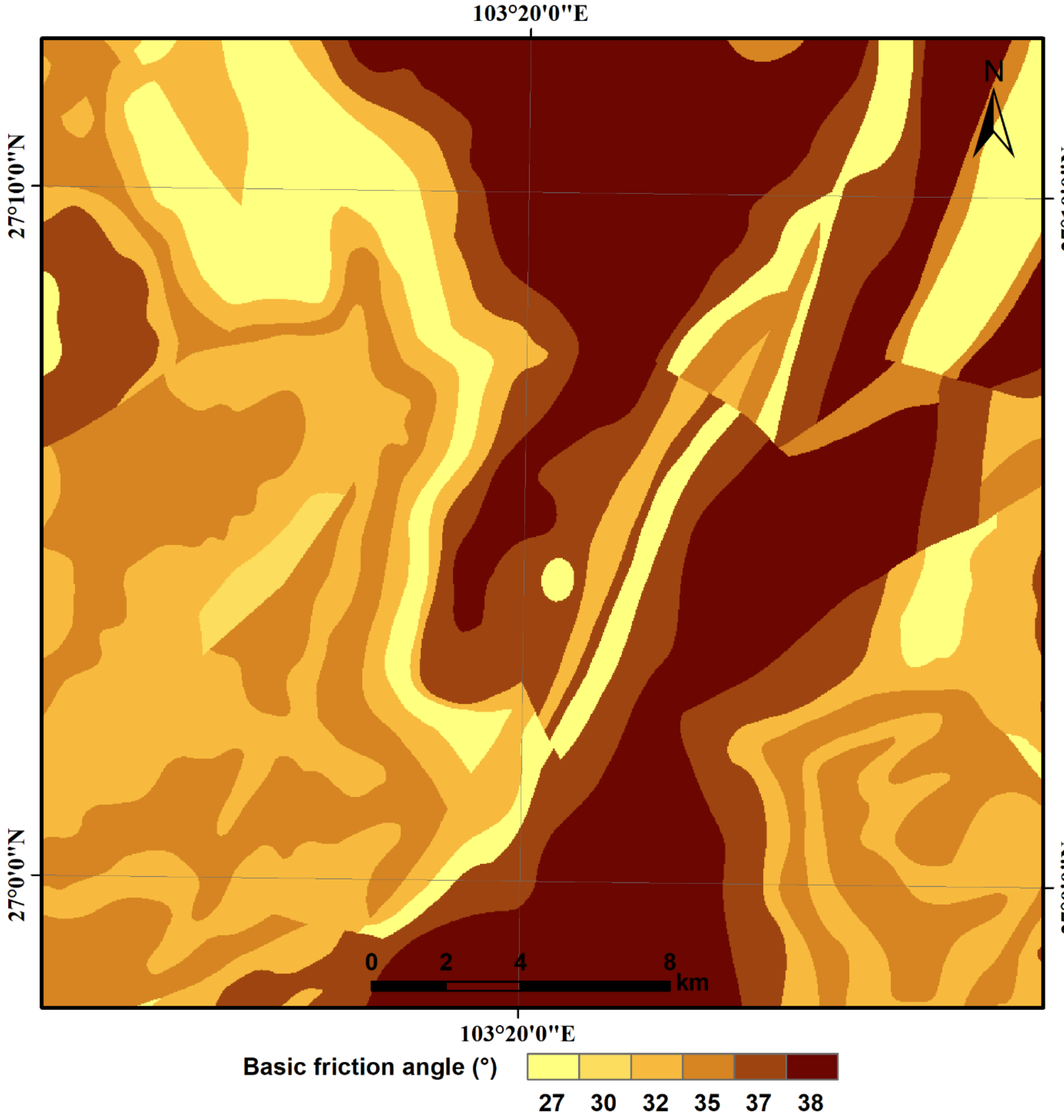

533

534 **Fig. 7.** Basic-friction-angle (ϕ_b) component of shear strength assigned to rock types in the study area.

535

https://doi.org/10.5194/nhess-2019-274
Preprint. Discussion started: 24 October 2019

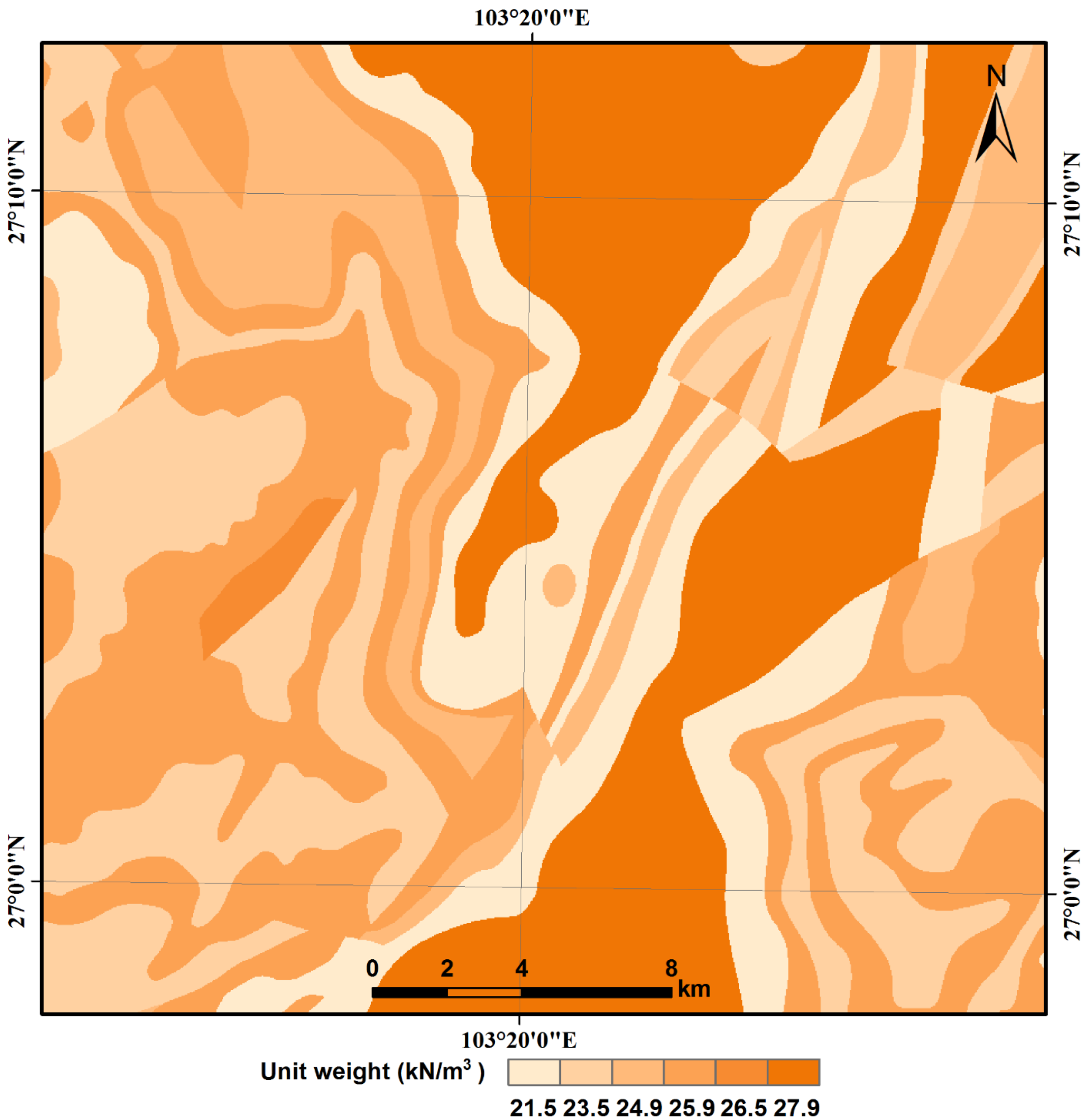

536

537 **Fig. 8.** Unit weight (γ) assigned to rock types in the study area.

538

https://doi.org/10.5194/nhess-2019-274
Preprint. Discussion started: 24 October 2019

Natural Hazards and Earth System Sciences Discussions

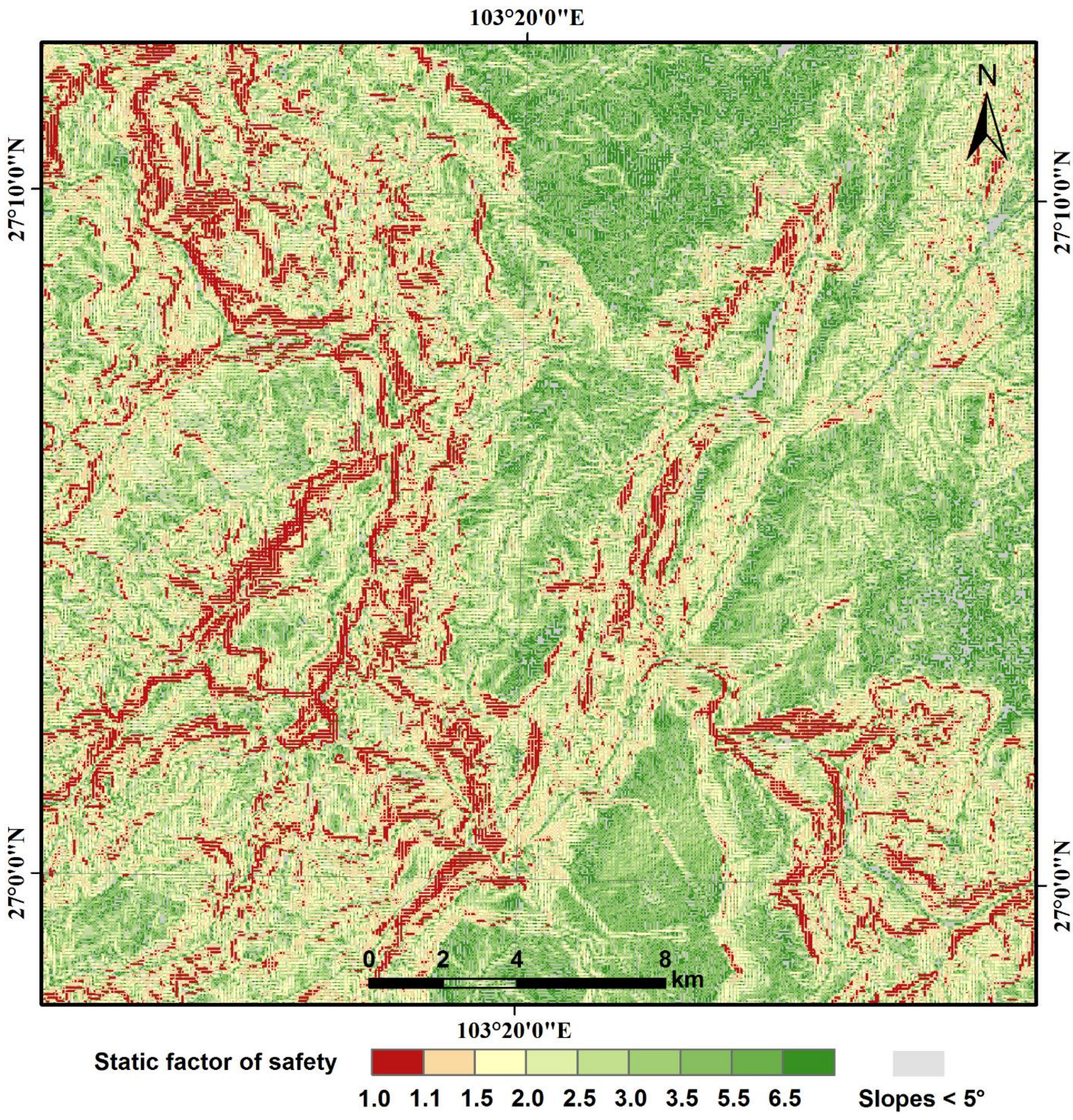

Fig. 9. Static factor-of-safety map of the study area.

https://doi.org/10.5194/nhess-2019-274
Preprint. Discussion started: 24 October 2019

Natural Hazards and Earth System Sciences
Discussions

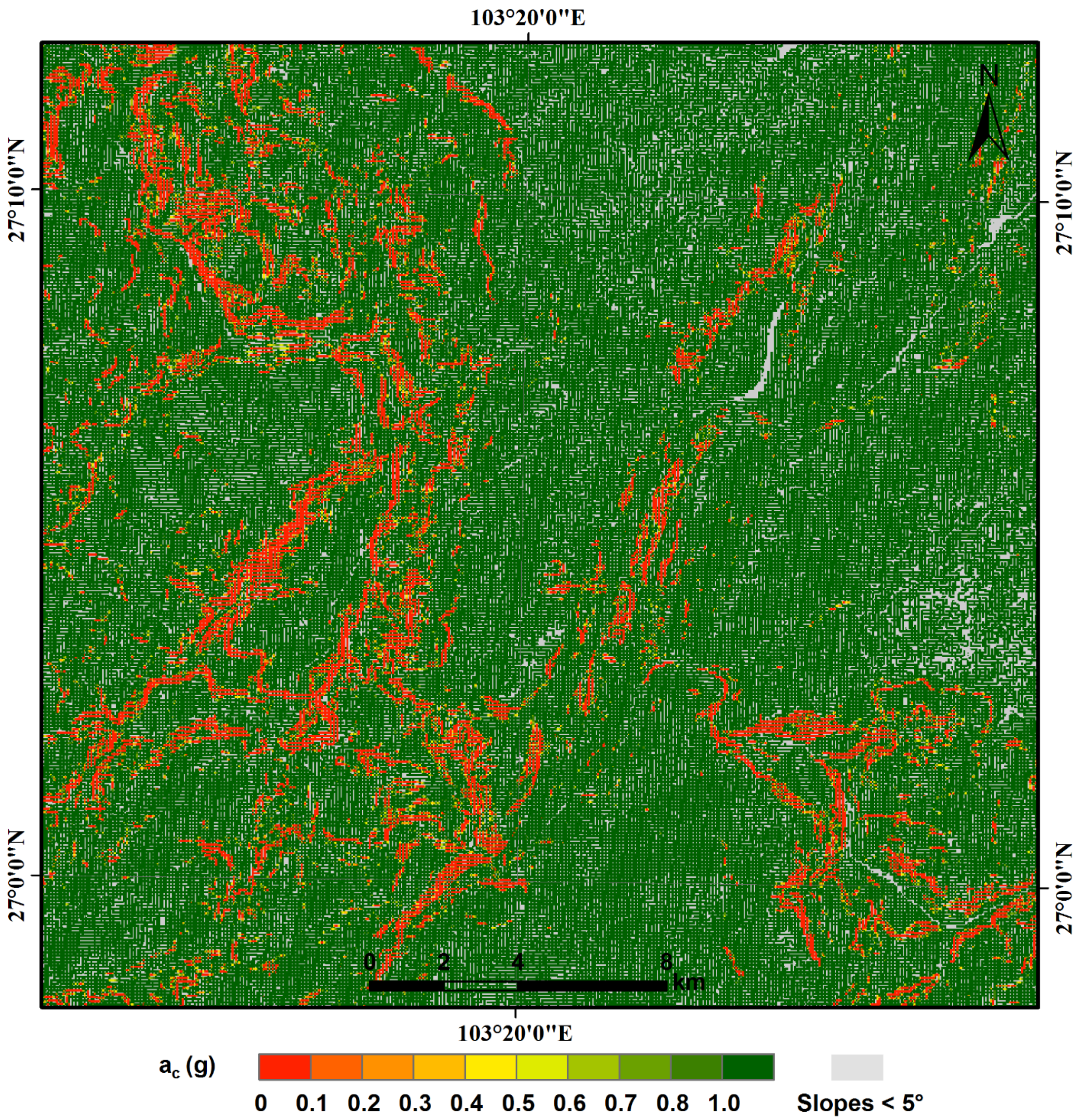

542

543 **Fig. 10.** Map showing critical accelerations in the study area.

544

https://doi.org/10.5194/nhess-2019-274
Preprint. Discussion started: 24 October 2019

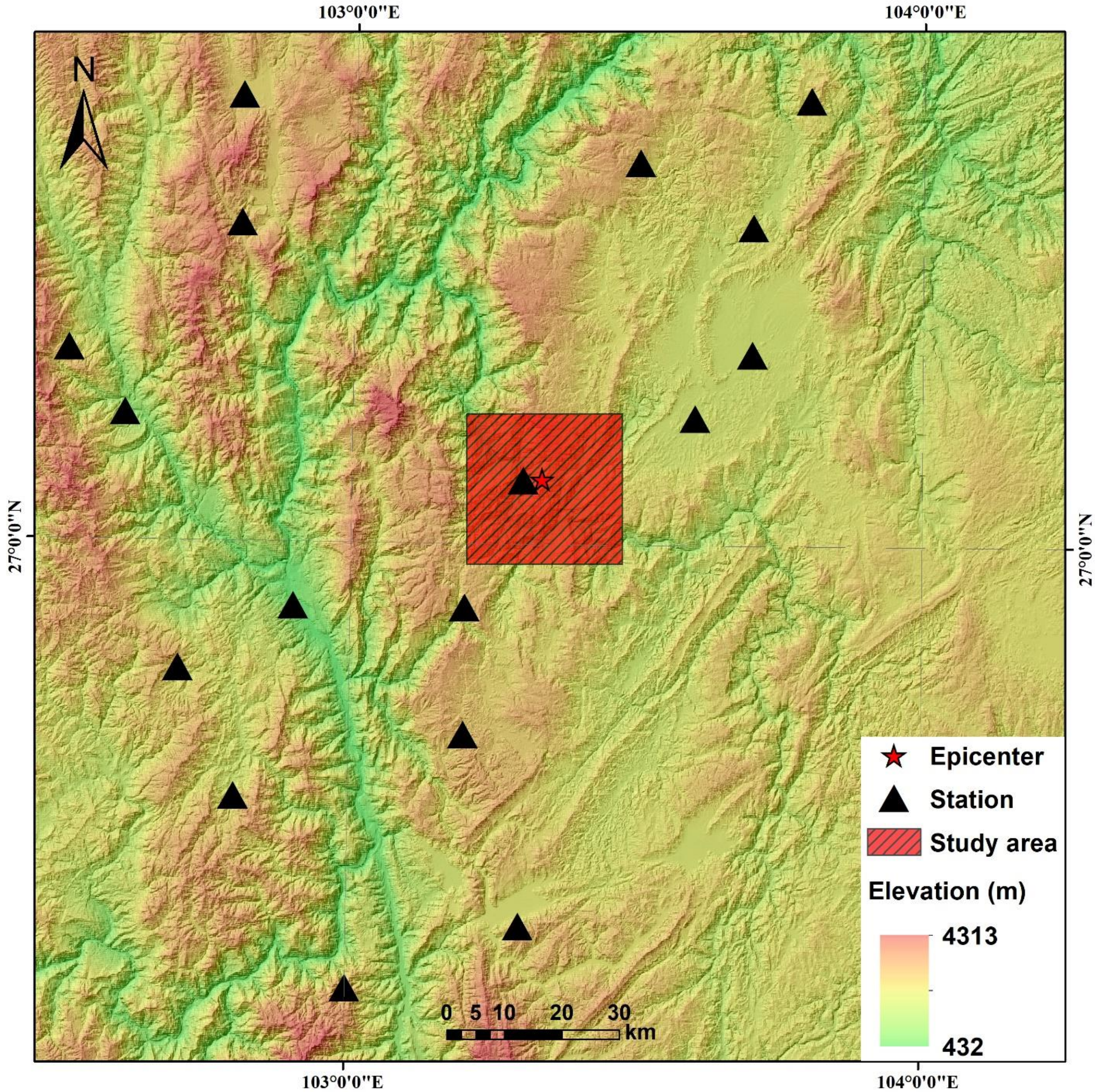

Fig. 11. Locations of strong-motion stations.

https://doi.org/10.5194/nhess-2019-274
Preprint. Discussion started: 24 October 2019

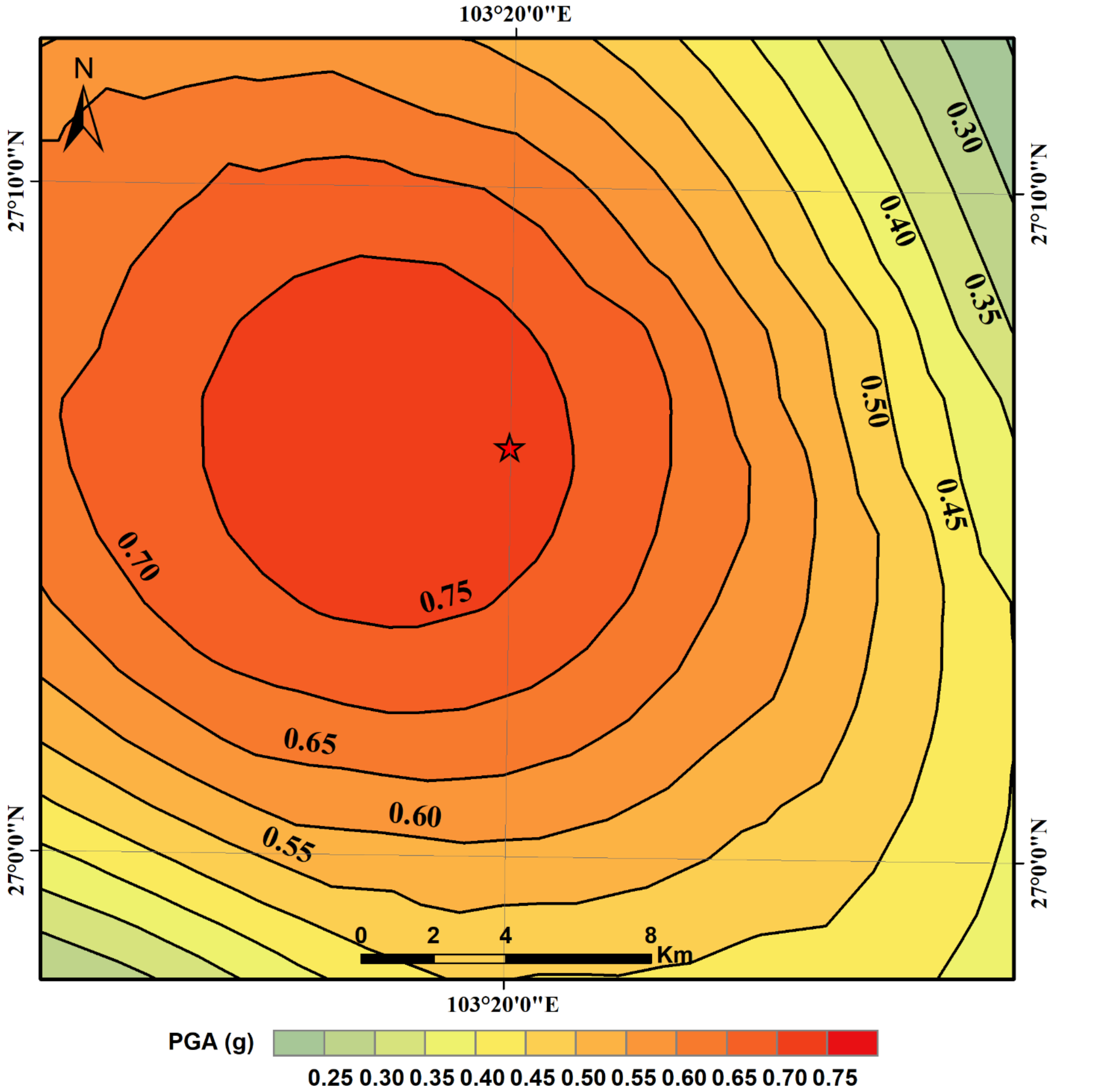

Fig. 12. Contour map of peak ground acceleration (PGA) produced by the Ludian earthquake in the study area. PGA values shown are in g.

https://doi.org/10.5194/nhess-2019-274
Preprint. Discussion started: 24 October 2019

Natural Hazards and Earth System Sciences
Open Access
EGU
Discussions

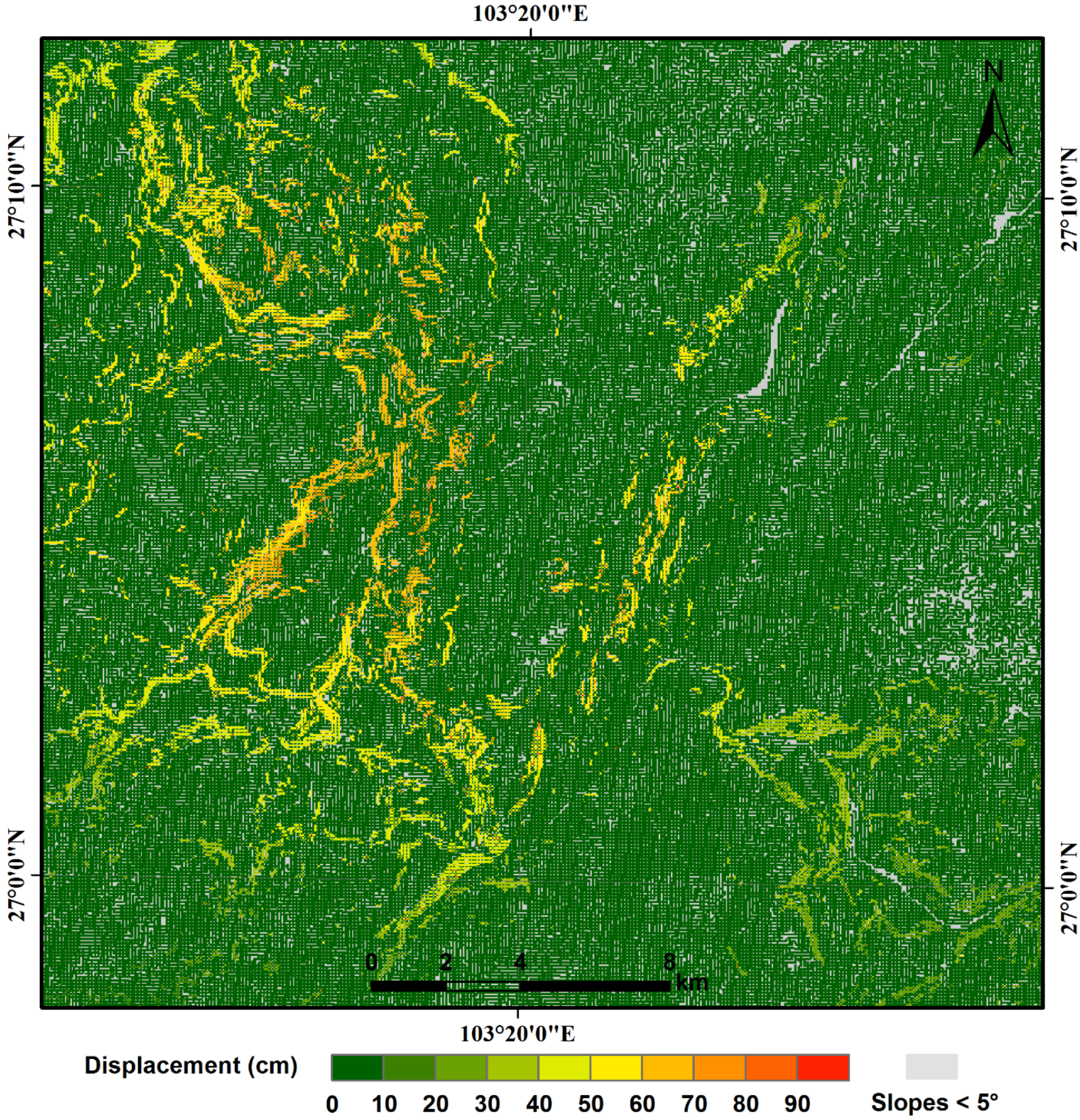

Fig. 13. Map showing predicted displacements in the study area.

Natural Hazards and Earth System Sciences
Open Access
EGU
Discussions

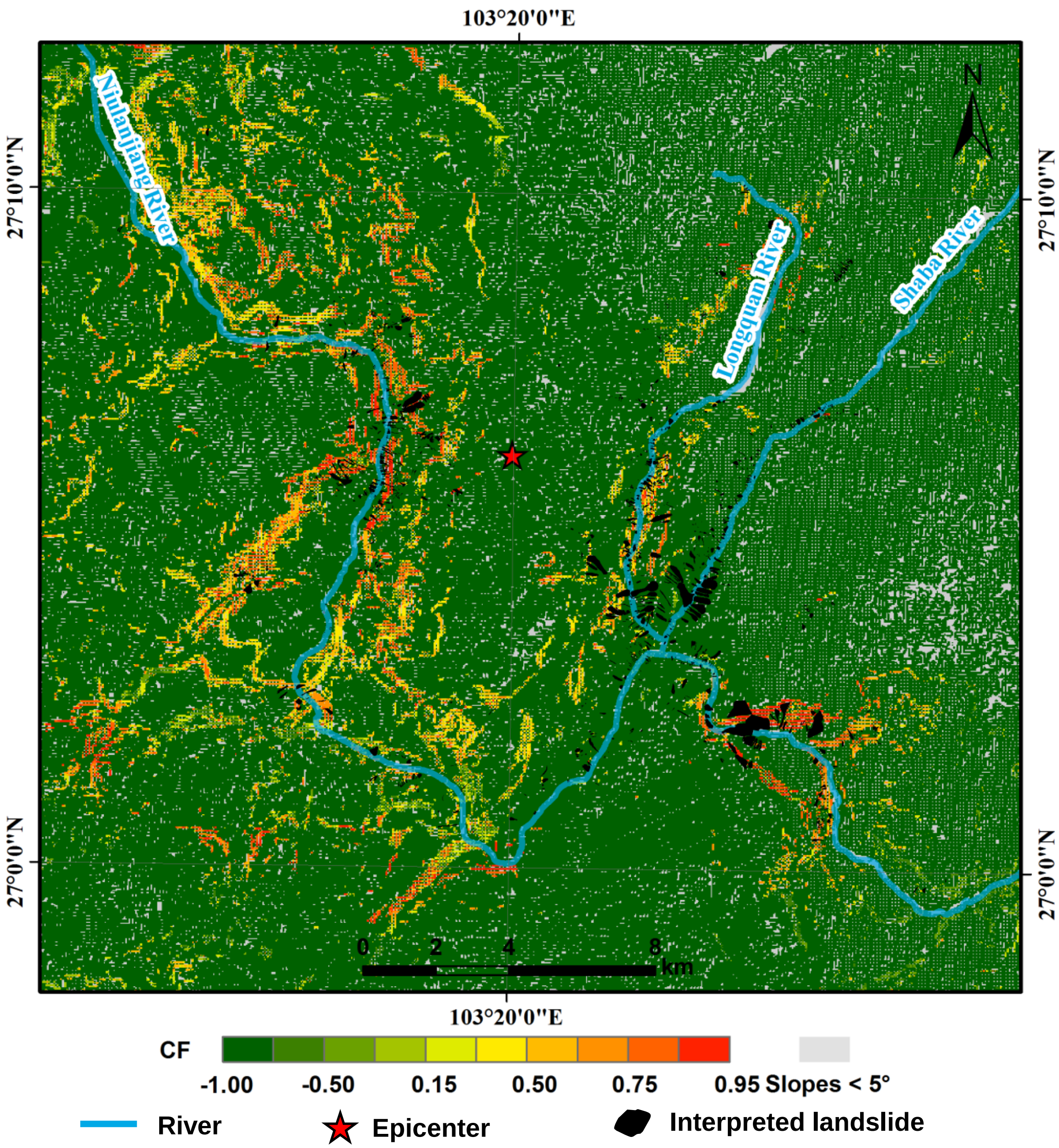

Fig. 14. Map showing confidence levels of coseismic landslides in the Ludian earthquake using method introduced in this paper. Confidence levels are portrayed in terms of values of *CF*.

https://doi.org/10.5194/nhess-2019-274
Preprint. Discussion started: 24 October 2019

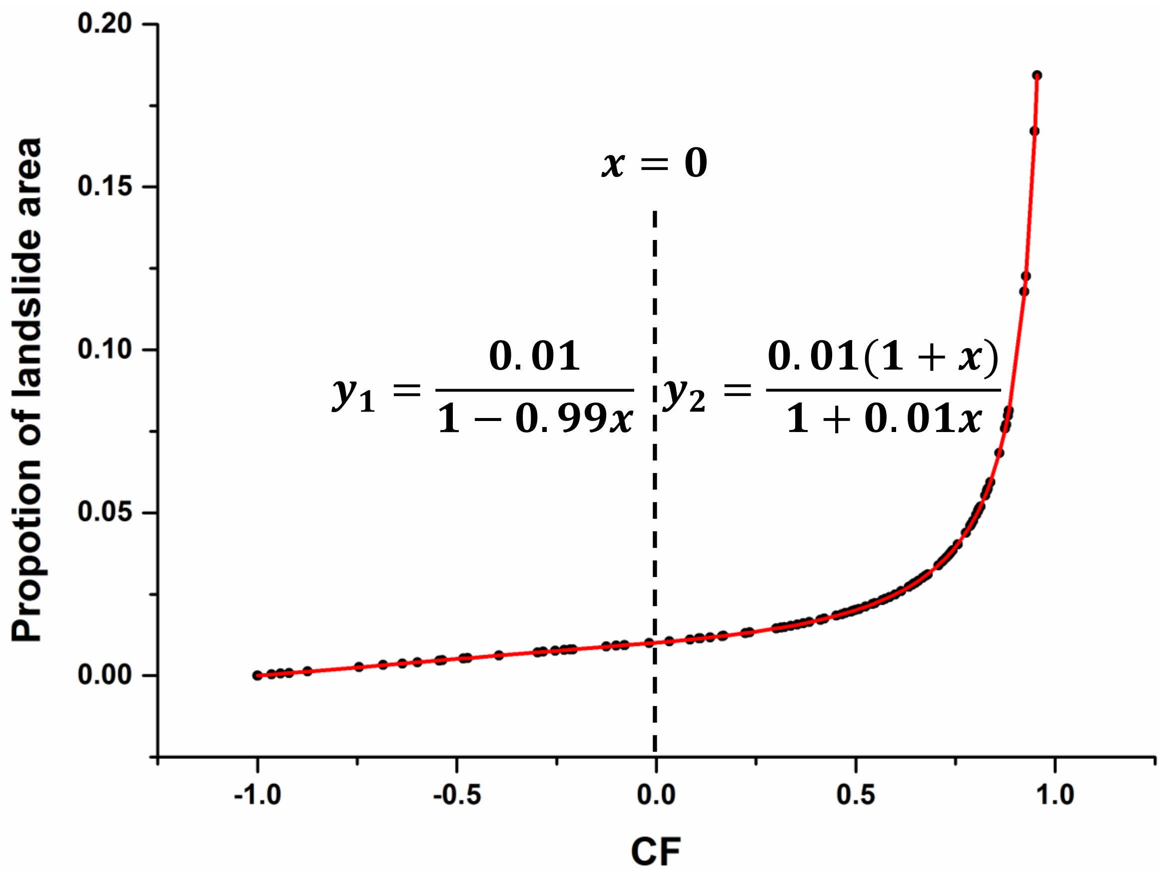

Fig. 15. Proportion of the area of landslides lying in each CF-value area. A dot shows the proportion of landslide area within an area of CF value; the red line is the fitting curve of the data using second order exponential growth function.

Natural Hazards and Earth System Sciences
Open Access
EGU
Discussions

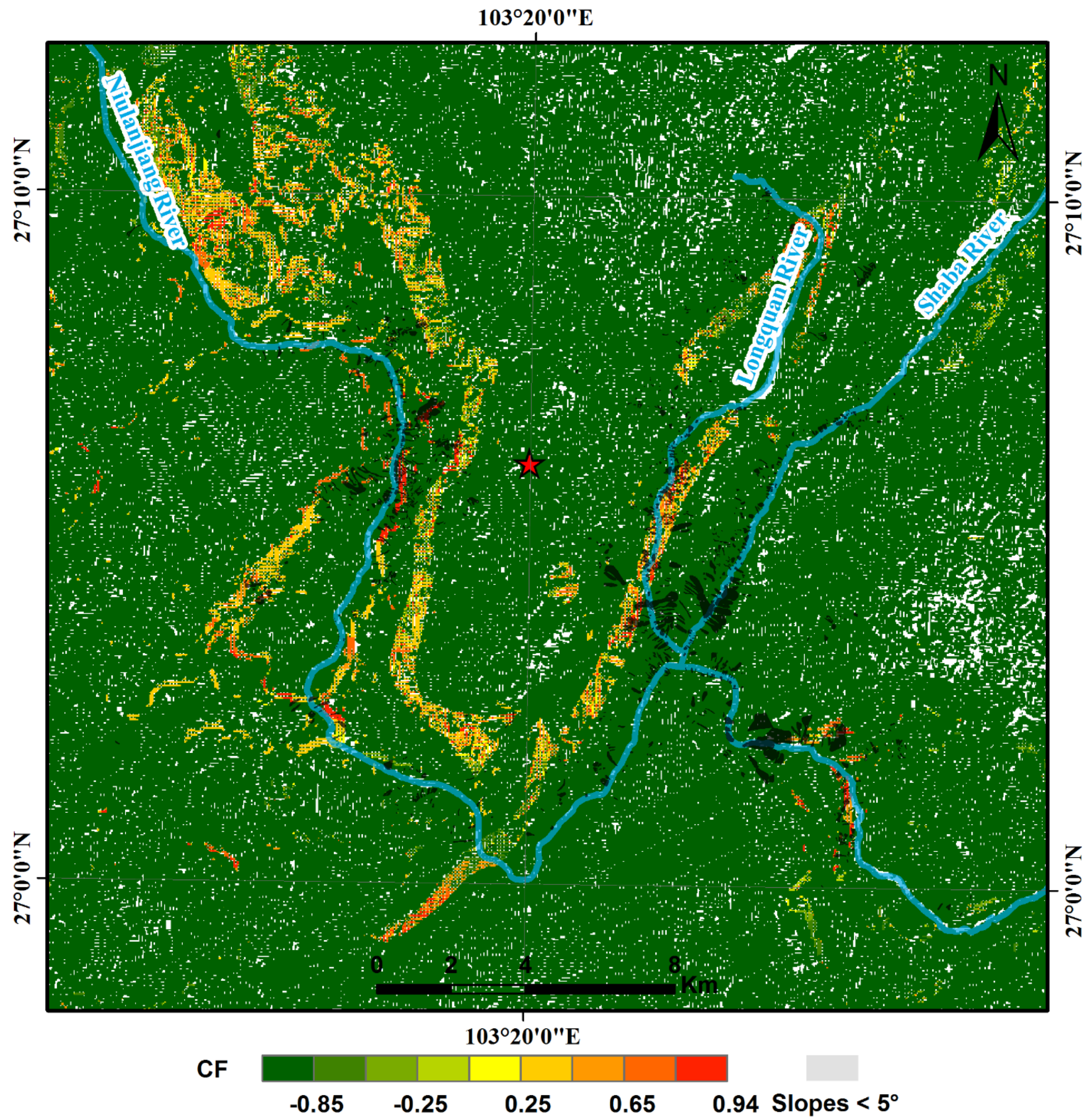

Fig. 16. Map showing confidence levels of coseismic landslides in the Ludian earthquake using a conventional Newmark analysis. Confidence levels are portrayed in terms of values of *CF*.

https://doi.org/10.5194/nhess-2019-274
Preprint. Discussion started: 24 October 2019

Natural Hazards and Earth System Sciences
Discussions

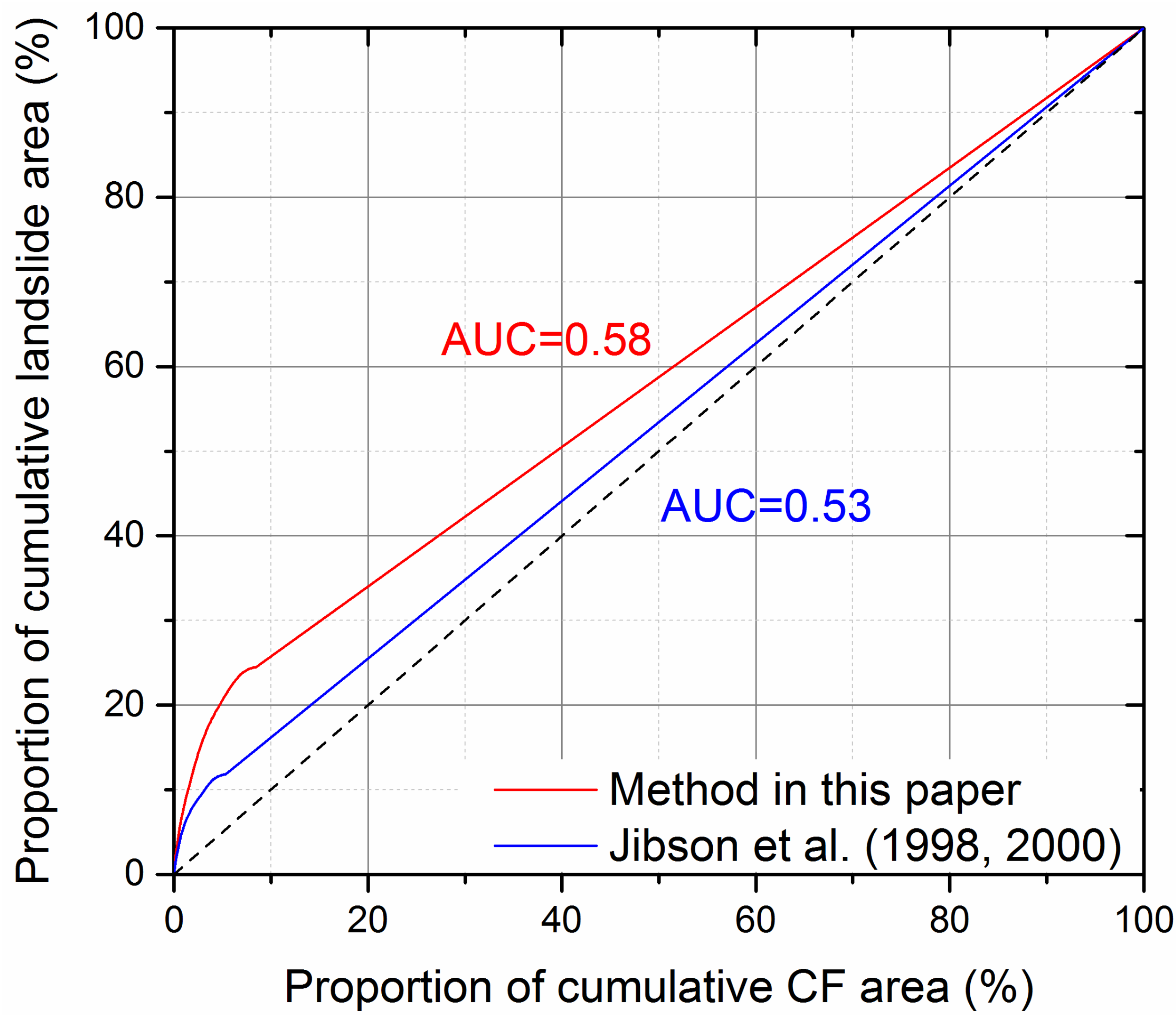

Fig. 17. Area under the curve plots for comparing the new method with a conventional Newmark's method.

https://doi.org/10.5194/nhess-2019-274
Preprint. Discussion started: 24 October 2019

Table Captions

Table 1. Shear strengths assigned to rock types in the study area.

Table 2. Station records included three components of the peak ground acceleration.

https://doi.org/10.5194/nhess-2019-274
Preprint. Discussion started: 24 October 2019

Natural Hazards and Earth System Sciences Discussions

Table 1

Shear strengths assigned to rock types in the study area.

Rock type	γ (kN/m^3)	ϕ_b	JCS_0 (MPa)	JRC_0	φ	c (kPa)	References
Dolomite	25.9	32°	140	9.5	43°	35	Singh et al., 2012 Giusepone, 2014 Alejano et al., 2014
Limestone	21.5	37°	160	9	45°	30	Bandis et al., 1983 Singh et al., 2012 Yong et al., 2018
Shale	24.9	27°	75	8	27°	16	Barton and Choubey, 1977 Bilgin and Pasamehmetoglu, 1990
Sandstone	23.5	35°	100	6	42°	24	Coulson, 1972 Bandis et al., 1983 Priest, 1993
Basalt	27.9	38°	205	8.5	50°	40	Coulson, 1972 Barton and Choubey, 1977 Alejano et al., 2014
Slate	26.5	30°	175	3	40°	11	Coulson, 1972 Barton and Choubey, 1977 Bandis et al., 1983 Alejano et al., 2012 Yong et al., 2018

Internal friction angle (φ), cohesion (c) and unit weight (γ) are derived from Geological Engineering Handbook (Geological Engineering Handbook Editorial Committee, 2018)

https://doi.org/10.5194/nhess-2019-274
Preprint. Discussion started: 24 October 2019

Table 2

Station records included three components of the peak ground acceleration.

No.	Station	Epicentral distance (km)	EW (g)	NS (g)	UD (g)	Average of horizontal components (g)
1	Longtoushan 1	8.114	0.5141	0.9679	0.7193	0.7410
2	Longtoushan 2	8.3	0.9685	0.7203	0.5147	0.8444
3	Qianchang	18.6	0.1490	0.1432	0.0539	0.1461
4	Ciyuan	32.6	0.0468	0.0457	0.0265	0.0463
5	Mashu	38.5	0.1380	0.1361	0.0663	0.1370
6	Qiaojia	43	0.0253	0.0210	0.0135	0.0232
7	Zhaotong 1	47.4	0.0096	0.0152	0.0065	0.0124
8	Zhaotong 2	47.671	0.0065	0.0096	0.0088	0.0081
9	Huidongxijie	63.3	0.0123	0.0128	0.0037	0.0126
10	Maolin	64.4	0.0251	0.0184	0.0111	0.0217
11	Yongshanmaolin	65.647	0.0111	0.0252	0.0184	0.0182
12	Jingan	66.2	0.0103	0.0122	0.0062	0.0113
13	Butuotuojue	66.8	0.0118	0.0173	0.0079	0.0146
14	Zhaotongjingan	67.392	0.0062	0.0103	0.0122	0.0083
15	Huidongqianxin	67.4	0.0224	0.0223	0.0067	0.0224
16	Ningnansongxin	69.2	0.0062	0.0081	0.0032	0.0071
17	Pugebaishui	76	0.0152	0.0149	0.0066	0.0151
18	Huize	76.5	0.0164	0.0182	0.0090	0.0173
19	Pugediban	81.2	0.0186	0.0127	0.0046	0.0156
20	Butuodiban	83.7	0.0024	0.0021	0.0024	0.0023
21	Tuobuka	85.2	0.0168	0.0168	0.0136	0.0168

https://doi.org/10.5194/nhess-2019-274
Preprint. Discussion started: 24 October 2019

Natural Hazards and Earth System Sciences
Discussions

22	Pugeyangwo	91.4	0.0066	0.0069	0.0022	0.0068
23	Daguan	91.8	0.0043	0.0035	0.0027	0.0039